ANL/LWRS-24/3

Light Water Reactor Sustainability Program

Performance Testing of Additively Manufactured 316L Stainless Steel in Light Water Reactor Environment

B. Alexandreanu, Y. Chen, and X. Zhang
Nuclear Science and Engineering Division, Argonne National Laboratory

September 2024

U.S. Department of Energy
Office of Nuclear Energy

ANL/LWRS-24/3

Performance Testing of Additively Manufactured 316L Stainless Steel in Light Water Reactor Environment

Nuclear Science and Engineering Division
Argonne National Laboratory

ANL/LWRS-24/3

Performance Testing of Additively Manufactured of 316L Stainless Steel in Light Water Reactor Environment

LWRS milestone Report Number: M3LW-24OR0402045

B. Alexandreanu, Y. Chen, and X. Zhang

Nuclear Science and Engineering Division, Argonne National Laboratory

September 2024

This page intentionally left blank

ABSTRACT

This report summarizes research activities conducted at Argonne National Laboratory in support of the development, qualification and certification of additively manufactured (AM) metallic components for the long-term sustainability of light water reactors. In this program, AM 316L stainless steel (SS) has been evaluated in light water reactor (LWR) environments for their fatigue, environmentally assisted fatigue, and stress corrosion cracking performances on specimens in as-printed condition, aiming for facilitating the regulatory acceptance and ultimately adoption of AM components in aging LWRs.

The performance of AM 316L in a light water environment was evaluated using AM-produced tubing - intended to act as surrogates for complex components where nuclear equipment vendors are more likely to consider AM technologies - printed at ANL using a Renishaw AM400 Laser Powder Bed Fusion (LPBF) system. The porosity of the as-built material was found to be small, 0.06%. Testing involved SCC initiation, SCC crack growth and EAF of the AM material in the as-built condition.

SCC CGR testing revealed that the fatigue and corrosion fatigue CGR response of two AM specimens in the as-built condition - oriented normal to and parallel to the build direction - was found to be similar to that expected for conventional alloys. Also, both AM specimens in the as-built condition proved to be extremely resistant to SCC. Crack initiation testing suggest that printing geometry affects local susceptibility to cracking, and that the as-printed surface initiated cracking faster than the machined surface.

Strain-controlled fatigue tests in air conducted with 3D-printed 316L SS under different strain amplitudes in a fully reversed mode revealed that the fatigue lives of AM 316L were slightly lower than that of traditionally made 316 SS, especially at high strain amplitude. For the tests performed in simulated PWR water, the fatigue lives of AM316L were lower than that obtained in air, suggesting a negative impact of LWR environment on AM materials. Cyclic softening dominated the evolution of stress amplitude for all fatigue tests on AM 316L SS both in air and in water. Following the same approach proposed in NUREG-6909 for wrought and cast austenitic SSs, environmental correction factors, F_{en}, were estimated for AM316L and were found to be reasonably close to those for conventional alloys, suggesting a similar baseline behavior in air for wrought and AM316L SSs.

TABLE OF CONTENTS

LIST OF FIGURES

LIST OF TABLES

ABBREVIATIONS

AM	Additive Manufacturing
AMMT	Advanced Materials and Manufacturing Technologies
ANL	Argonne National Laboratory
APS	Advanced Photon Source
ASME	American Society of Mechanical Engineers
ASTM	American Society for Testing and Materials
CT	Compact Tension
DOE	Department of Energy
EAF	Environmental Assisted Fatigue
JSME	Japanese Society of Mechanical Engineers
LPBF	Laser Powder Bed Fusion
LWR	Light Water Reactor
LWRS	Light Water Reactor Sustainability
NRC	Nuclear Regulatory Commission
ORNL	Oak Ridge National Laboratory
SAM	Strain Amplitude
SCC	Stress Corrosion Cracking
SS	Stainless Steel
CGR	Crack Growth Rate

ACKNOWLEDGMENTS

This research was supported through the U.S. Department of Energy's Light Water Reactor Sustainability program, Materials Research Pathway. Materials Research Pathway lead: Dr. Xiang (Frank) Chen.

This research used resources of the Advanced Photon Source, a U.S. Department of Energy Office of Science User Facility operated for the DOE Office of Science by Argonne National Laboratory under Contract no. DE-AC02-06CH11357.

The authors gratefully acknowledge the assistance of E. Listwan and J. Listwan in specimen preparation, test set-up and printer operation, JS. Park, P. Kenesei and J. Almer in synchrotron X-ray beamtime experiment, A. Tekawade, P. Kenesei, C. Chuang, Y. Satapathy and C. Carter in synchrotron X-ray tomography data analysis. Additionally, the authors would also like to express their gratitude to D. Gandy and S. Tate from the Electric Power Research Institute for supplying a stainless steel 316L flange coupon for testing.

.

1 Introduction

Nuclear power has been the largest source of carbon-free power in the U.S. (and much of the developed world) for almost a half century [1]. As such, in the U.S. today, nuclear power plants of the Light Water Reactor (LWR) design generate ~20% of all electricity, comprising over half of carbon-free electricity generation [2]. In order to meet the short-term 2030 greenhouse gas emission reduction target, the existing nuclear fleet will play an important role [3]. Specifically, extending the operating lives of the existing nuclear reactors, and their continued operation are important opportunities to leverage this firm, carbon-free source of power. EPRI estimates that extending the operating life of the existing nuclear fleet to 80 years will result in a 106% increase in power generation when compared to the current remaining operational licenses [3]. Nevertheless, the extended operating lives will pose new challenges to materials and the fabrication of replacement components.

Metal additive manufacturing (AM) or 3D printing by laser powder bed fusion (LPBF) has the potential to transform the nuclear industry by producing high quality, custom-designed components faster and cheaper, thus helping with extending the operating life and enhancing the performance of the current plants [4,5,6]. However, a lack of clarity on the qualification, standards and regulatory pathways for AM fabricated nuclear components is a potential obstacle to their use. The US Nuclear Regulatory Commission (NRC) staff has indicated they expect to approve components using a performance-based approach [7] and that, for a material exposed to a LWR environment, the performance-based approach would include the evaluation of environmental effects such as corrosion, stress corrosion cracking (SCC), and environmental fatigue [7,8].

Type 316 austenitic stainless steel has been widely used in various types of LWRs, hence, it has been an early candidate for AM development. One of the initial and most comprehensive studies attempting to evaluate the performance of AM 316L in LWR environment was conducted by X. Lou et al. [9, 10]. The authors commissioned AM samples as well as post-built treatments designed to reduce porosity in the AM material from an external vendor. The authors found that Hot Isostatic Pressing (HIP) + Solution Annealing (SA) reduces porosity from 0.19% in the stress-relieved only alloy to 0.08%. While SCC testing in water involved both as-built (and heat treated) specimens and 20% cold-worked (post post-build treatment) specimens, the latter were emphasized as a means of accelerating the SCC tests. The authors found that, after proper high temperature annealing, AM 316L SS by LPBF exhibits similar SCC growth behavior as its wrought counterpart.

This report summarizes research activities initiated at Argonne National Laboratory in support of the development, qualification and certification of additively manufactured (AM) metallic components to allow for innovative reactor design and licensing. The approach undertaken in this study is different from those of the previous studies in several ways. First, the geometry of the AM-built samples was chosen to be close to that of a component used in a nuclear plant. For example, two SS 316L pieces of tubing – surrogates for component-like structures – were built using LPBF AM at ANL. Additional materials – a flange sector build by Westinghouse – was obtained from EPRI. Second, the initial investigation and testing of these materials focused on the as-built structures, as post-built treatments are not always available or feasible for all components. For this research, a microstructural investigation - with a focus on porosity - of the as-built structures was conducted, as well as

mechanical testing with a focus on cracking by fatigue, corrosion fatigue, and stress corrosion cracking (SCC) in a LWR environment. The results were compared with the known behavior of conventionally-produced alloys.

Chapter 2 describes the alloys used in this study and the experimental facilities used to carry out the performance testing in LWR environment. For this purpose, two AM 316L tubes - intended to act as surrogates for complex components where nuclear equipment vendors are more likely to consider AM technologies – were printed at ANL using a Renishaw AM400 LPBF system. A microstructural evaluation – with an emphasis on porosity – was conducted. The crack growth testing equipment and experimental approach as well as the Environmental Fatigue apparatus are presented. ANL generally followed a well-established testing protocol that has been employed for a number of years and was reported in previous ANL reports.

Chapter 3 provides findings of the microstructural examinations and the results of the environmentally assisted fatigue (EAF) testing and crack initiation and crack growth rate (CGR) tests of AM 316L in a light water reactor environment. Complete CGR data sets are provided as a function of testing conditions, and presented as crack advance vs. time plots. The corrosion fatigue and stress corrosion cracking (SCC) crack growth rate response was evaluated in simulated primary coolant, and the results were compared to those obtained on conventionally-produced alloys. Fatigue lives in air and in LWR environment were obtained at different strain amplitudes and compared with those of wrought SSs.

Chapter 4 provides a discussion of the testing results in the framework provided by the well-established fatigue and corrosion fatigue behavior for these alloys, as well as the industry-proposed disposition curves for crack growth [11]. Following the approach previously developed for wrought and cast SSs, the environmental effect on fatigue life was accounted for with a correction factor.

Finally, Chapter 5 gives a summary of the main findings and conclusions.

2 Experiment

2.1 Alloys

2.1.1 Alloy 316L tubing produced at ANL

Two AM 316L tubes intended to act as surrogates for complex components where nuclear equipment vendors are more likely to consider AM technologies, Figure 1, were printed using a Renishaw AM400 LPBF system. The printing parameters are also included in the figure. The chemical composition (wt.%) of SS 316L powder are given in Table 1.

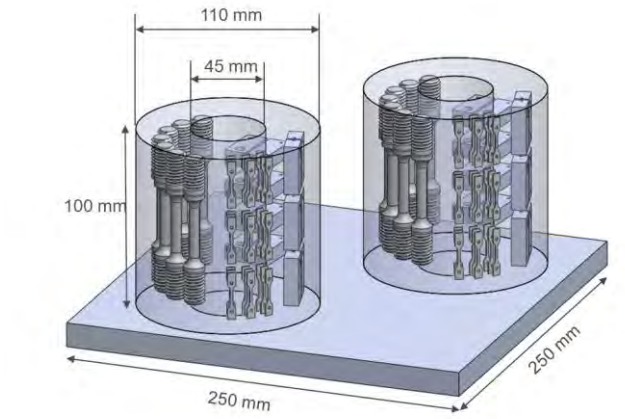

(a)

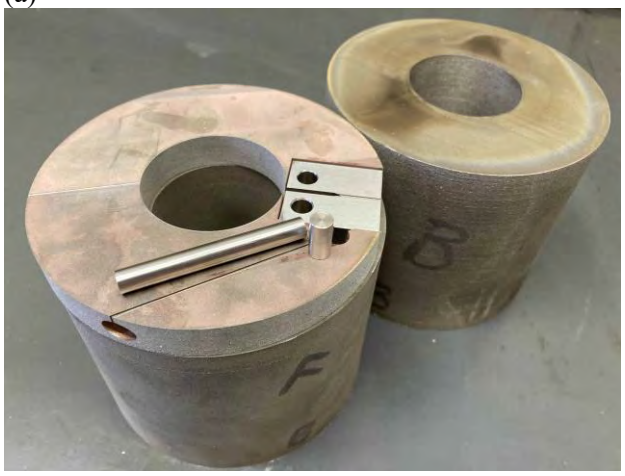

(b)

Parameter	Value
Laser Power	195 W
Layer Thickness	50 µm
Melting Method	Stripe (5mm)
Rotation	67 degrees
Exposure Time	80 µs
Point Distance	60 µm
Effective Velocity	0.75 m/s
Hatch Spacing	110 µm
Energy Density	53.33 J/mm^3
Recoater Blade	Rubber
Atomization Gas	Argon
Build Chamber Atmosphere	Argon
Equipment Type	Renishaw AM400

(c)

Figure 1 AM SS 316L tubing (a) as planned, and (b) as printed, with compact tension (CT) specimen for SCC CGR testing in LWR environment. (c) print parameters.

Table 1 Chemical composition (wt.%) of SS 316L powder and deposited alloy

Alloy	Analysis	C	Mn	Fe	S	P	Si	Cu	Ni	Cr	Mo	Ti	Nb	Co
Powder	Vendor	0.022	0.90	Bal.	0.005	0.008	0.69	-	12.6	17.9	2.43	-	-	-
AM part	Luvak Inc.	0.017	0.57	67.29	0.009	0.013	0.59	0.12	12.33	16.55	2.26	-	-	0.058

2.1.2 Compact tension (CT) specimens produced at ANL

Compact tension (CT) specimens were printed in order to allow for an evaluation of the crack initiation in AM 316L, Figure 2. The specimens were printed using the Renishaw AM400 LPBF system, with the parameters listed previously. The compositions (wt. %) of SS 316L powder and the AM part are given in Table 1.

Figure 2 CGR/crack initiation compact tension specimens printed using the Renishaw AM400 LPBF system.

2.1.3 Material produced by industry

A sector from an AM 316L flange produced by Westinghouse Electric Company (WEC) and used to generate mechanical property data in air for the ASME code case # 20-254 was received from EPRI, Figure 3. Specimens from this flange will be used by ANL to generate the "performance" data in LWR environment (EAF and SCC) needed for the regulatory acceptance of the code case.

Figure 3 AM 316L flange produced by WEC and used to generate mechanical property data in air for the ASME code case # 20-254 was received from EPRI.

Both CGR/crack initiation and fatigue specimens were machined from the flange according to schematic shown in Figure 4.

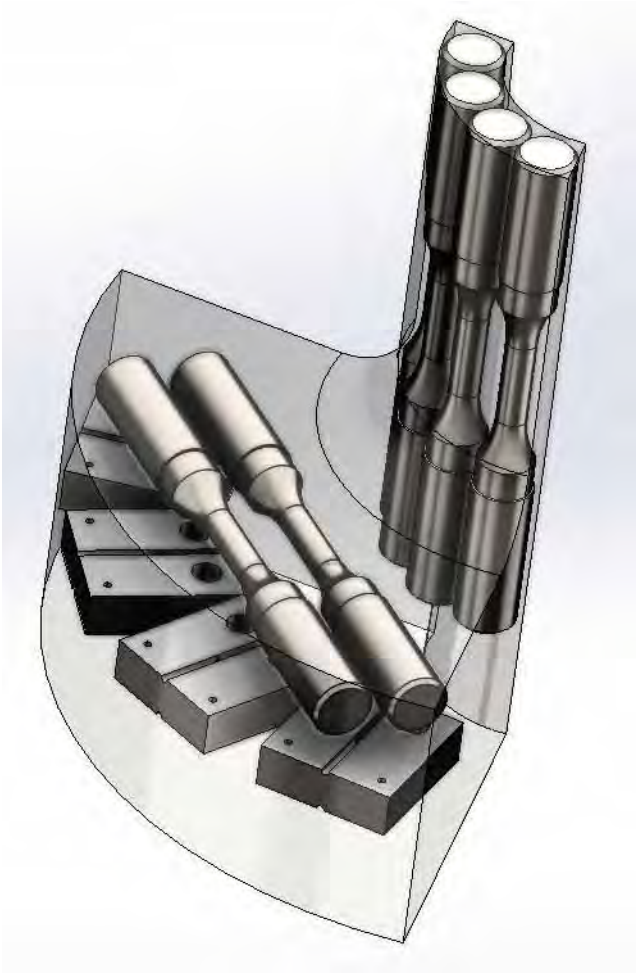

Figure 4 CGR/crack initiation and fatigue specimens were machined from the AM 316L flange produced by WEC and received from EPRI.

2.2 Mechanical testing in LWR environment

2.2.1 SCC CGR testing

The tests conducted under this project were performed on ½-T compact tension (CT) specimens; the geometry of the CT specimens is shown in Figure 5. The CGR tests were conducted in simulated PWR environments at 320°C. The testing protocol was in accordance with ASTM E-647, "Standard Test Method for Measurement of Fatigue Crack Growth Rates," [12] and ASTM E-1681, "Standard Test Method for Determining a Threshold Stress Intensity Factor for Environment-Assisted Cracking of Metallic Materials under Constant Load" [13].

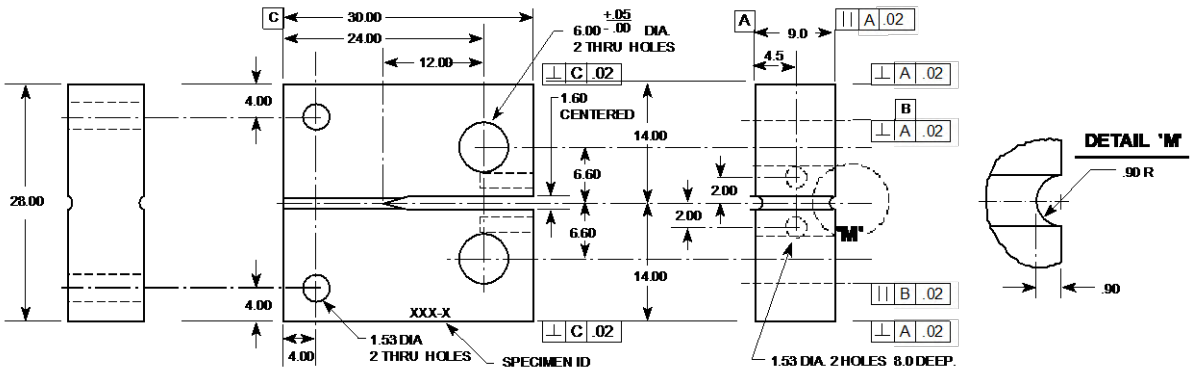

Figure 5 Configuration of the ½-T CT specimen used for this study. Dimensions are in mm.

The CGR tests were conducted in test facilities equipped with either 2 or 6-liter stainless steel (SS) autoclaves. Each system has a suite of calibrated instrumentation, including digitally controlled hydraulic loading and load cells, and an independent water loop to maintain a simulated PWR environment with water chemistry monitoring. The test systems are nearly identical except for the maximum load rating of the test frame and the volume of the autoclave vessel. A detailed description of the test system with the 2-liter autoclave is provided in this section.

The 2-liter autoclave test facility allows test temperatures of up to 350°C. Figure 6 is a photograph showing the entire test system. The servo-hydraulic test frame consists of a load train, an autoclave support frame, and autoclave. The hydraulic actuator is mounted on bottom of the test frame, with the load train components located above it. The load cell is located at the bottom of the pull rod. An Instron Model 8800 system is used to control the load on the specimen. The test temperature is maintained by heater bands mounted on the autoclave body.

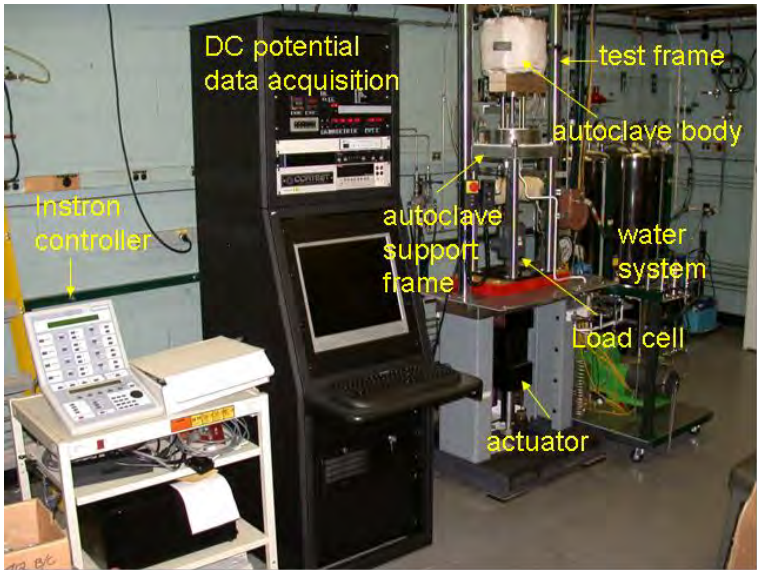

Figure 6 Layout of the 2-liter SCC test system.

The autoclave support frame consists of a thick plate supported by four compression rods (Figure 7). The internal load frame that contains the test specimen consists of a top plate supported by three rods. The upper two-piece clevis assembly is fastened to the top plate of the internal load frame, and the lower piece clevis assembly is connected to the pull rod. The specimen to be tested is mounted between the clevises. The specimen and clevises are kept electrically insulated from the load train by using oxidized Zircaloy pins and mica washers to connect the clevises to the rest of the load train. Water is circulated through a port in the autoclave head, which serves both as inlet and outlet. A schematic diagram of the recirculating water system is shown in Figure 8.

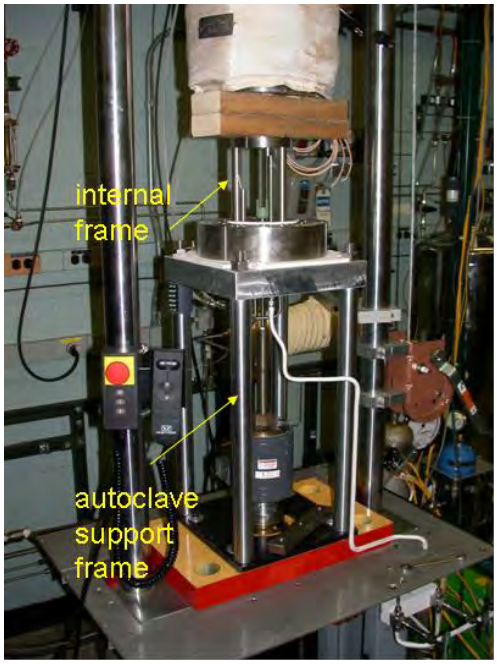

Figure 7 Photograph of the specimen load train for the 2-liter autoclave.

The simulated PWR feedwater contains 2 ppm Li as LiOH, 1000 ppm B as HBO_3, ≈2 ppm dissolved hydrogen (≈23 cm^3/kg), and less than 10 ppb dissolved oxygen (DO) [14]. Water is circulated at relatively low flow rates (15-25 mL/min). The test temperature was 320°C.

Crack extensions are monitored by the reversing-direct current (DC) potential difference method, Figure 9. In this method, a constant DC current is passed through the test specimen and the crack length is measured through the changes in the electrical voltage at the crack mouth. The electrical voltage measured across the crack mouth is related to the unbroken crack ligament resistance through the Ohm's law. Thus, as the crack advances, the length of the unbroken ligament decreases and its resistance increases. In short, as the crack advances the voltage measured across the crack mouth increases. Figure 9 shows a typical configuration of a CT specimen instrumented for crack growth measurements by the DC potential method: the current leads are welded on the top and bottom surfaces of the specimen, and potential leads are welded on the front face of the specimen across the machined notch but on diagonal ends. Also, to compensate for the effects of changes in resistivity of the material with time, an internal reference bar of the same material being tested is installed in series, near the test specimen. The voltage readings across the reference bar are used to normalize potential drop measurements for the CT test specimen. The changes in potential drop measurements for the CT test

specimen are transformed into crack advance data using correlations developed for the specimen geometry that is tested. In practice, voltage readings are taken successively as the current is reversed, and, typically, 800 voltage readings are needed to generate 1 crack advance data point, approximately every 4 min. with a resolution of approximately 1-2 µm [0.039-0.079 mils].

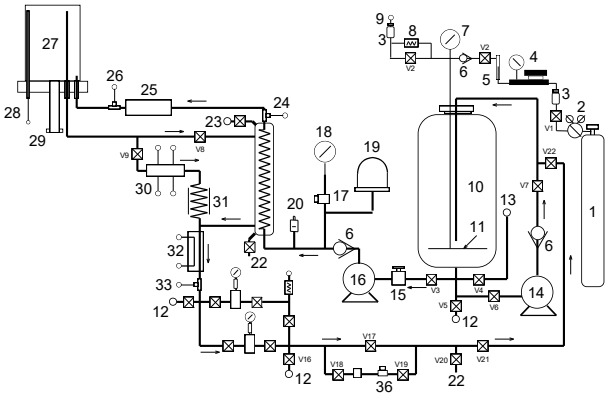

1. COVER GASS SUPPLY TANK
2. TWO-STAGE HIGH-PRESSURE REGULATOR
3. FLASH ARRESTOR
4. LOW-PRESSURE REGULATOR
5. FLOW METER
6. CHECK VALVE
7. COMPOUND VACUUM & PRESSURE GAUGE
8. PRESSURE RELIEF VALVE
9. VENT TO AIR & FLASH ARRESTOR
10. FEEDWATER STORAGE TANK
11. SPARGE TUBE
12. WATER SAMPLE PORT
13. FEEDWATER FILL PORT
14. FEEDWATER TANK RECIRCULATION PUMP
15. SOLENOID VALVE
16. HIGH-PRESSURE PUMP
17. PRESSURE TRANSDUCER
18. HIGH-PRESSURE GAUGE
19. ACCUMULATOR
20. RUPTURE DISC
21. HEAT EXCHANGER (HX)
22. DRAIN
23. SYSTEM BLEED PORT
24. HEAT EXCHANGER OUTLET TC
25. AUTOCLAVE PREHEATER
26. PREHEATER OUTLET TC
27. COMMERCIAL AUTOCLAVE
28. THERMOWELL
29. "BAL SEAL" RETAINER
30. ECP CELL
31. AIR-COOLED COIL
32. WATER COOLED HEAT EXCHANGER
33. BACK-PRESSURE REGULATOR (BPR) INLET TC
34. BPR
35. PH METER
36. CONDUCTIVITY METER

Figure 8 Schematic diagram of the recirculating 2-liter autoclave system.

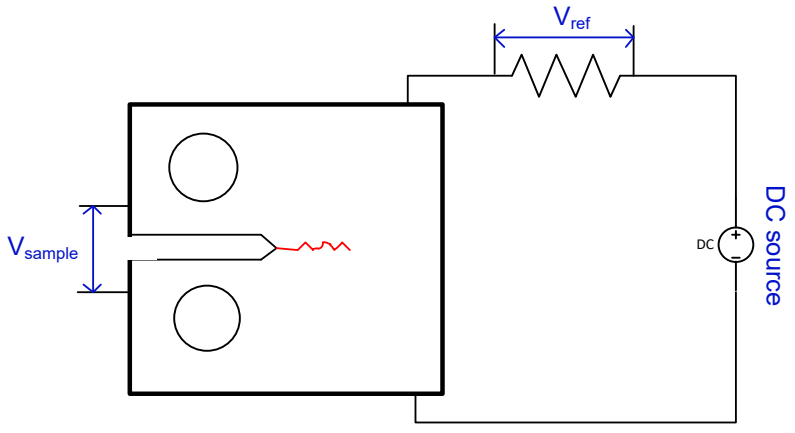

Figure 9 Principle of crack length measurement by the DC potential method.

2.2.2 SCC initiation testing

Crack initiation testing was conducted in the same facility used for SCC CGR testing with the purpose of evaluating the effect of surface finishing in crack initiation. For this, two printed AM316L specimens differing only at the notch – "as printed" vs. "machined" – were instrumented for DC potential and loaded simultaneously, Figure 10. To accelerate the degradation effect(s), the water environment was aerated (8 ppm DO).

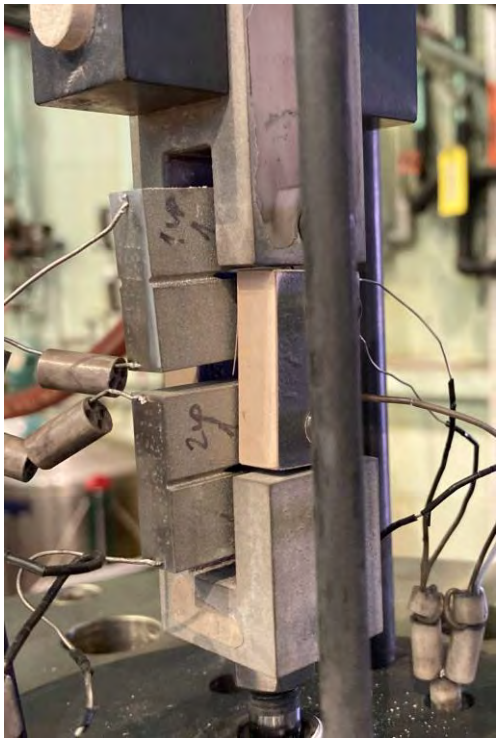

Figure 10 AM316L printed CT specimens differing only at the notch – "as printed" vs "machined"- instrumented for DC potential and loaded in series.

2.2.3 Fatigue and environmentally assisted fatigue testing

Two sample geometries were used in this study for fatigue tests conducted in air and in a LWR water environment (i.e., environmentally assisted fatigue, EAF). The sample used for the in-air fatigue tests has a nominal gauge diameter of 0.215" (5.46 mm), a gauge length of 0.64" (16.26 mm), and a total length of 4.0" (101.6 mm), as shown in Figure 11a. For the EAF tests however, a slightly smaller sample geometry was used due to the space limitations of the autoclave. As shown in Figure 11b, both the gauge diameter and length of the EAF sample were approximately 14% smaller than those of the in-air fatigue sample.

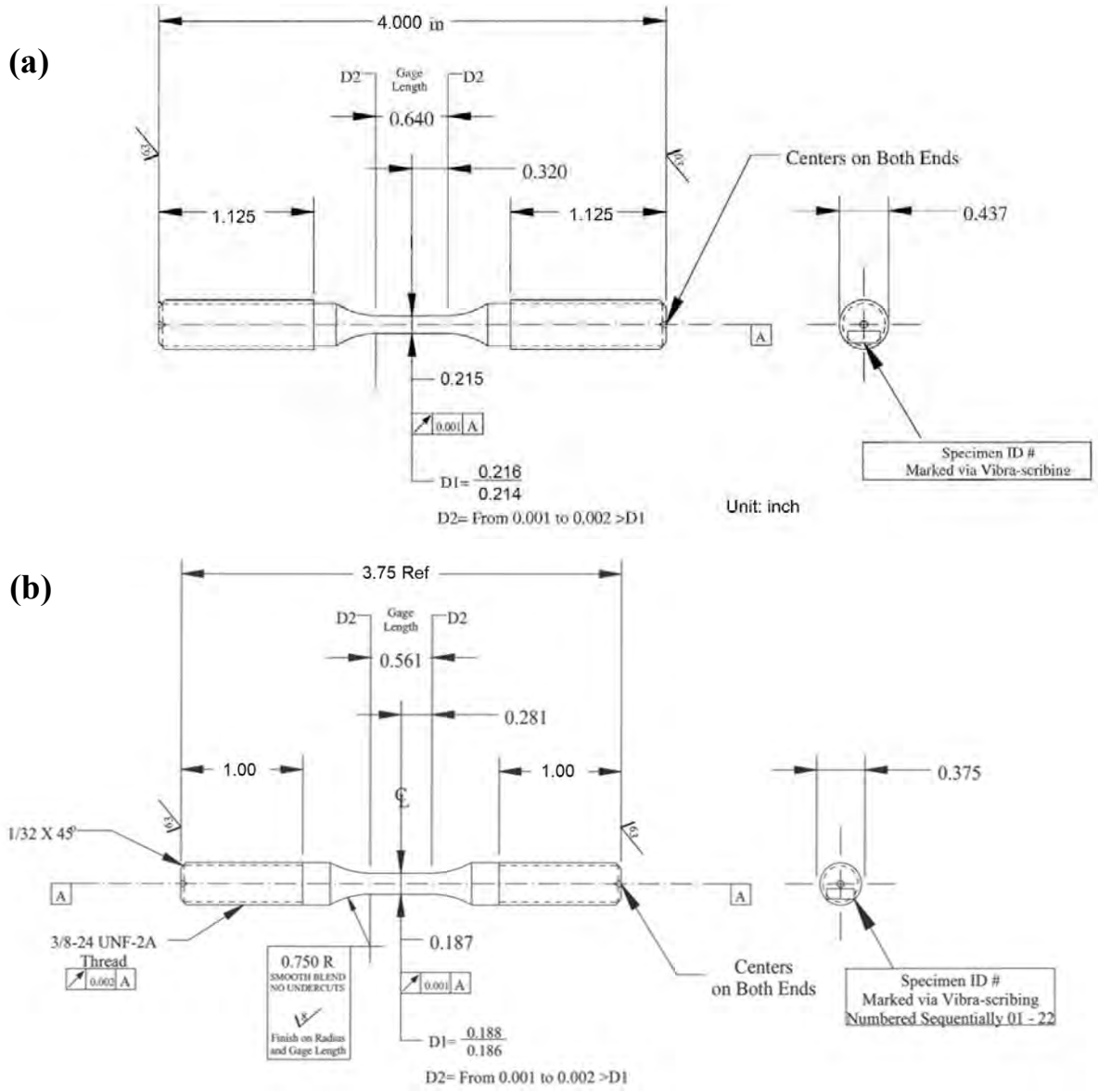

Figure 11 Schematics of the samples used for the in-air fatigue tests (a), and for the EAF tests in a LWR environment (b). Note that all dimensions in the drawings are in inch.

Both types of samples were extracted from the LPBF-printed 316L SS tubes. As shown in Figure 12, all samples were cut along the longitudinal direction of the printed tube – the build direction. The samples to be tested in air were extracted from the middle plane of the tube wall, while the samples to be tested in water were extracted from three circumferential planes evenly spaced from the tube's inner diameter (ID) and outer diameter (OD).

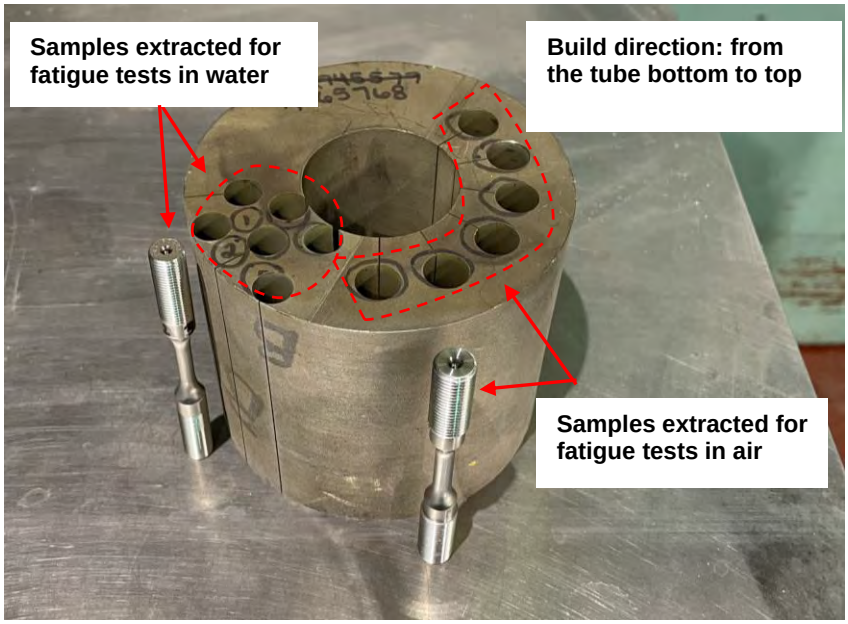

Figure 12 Locations where the fatigue and EAF samples were extracted from

Fatigue tests in air were performed per ASTM Standard E606/606M, "Standard Test Methods for Strain-Controlled Fatigue Testing." [15] The tests were carried out on a closed-loop servo-hydraulic test frame equipped with a three-zone split furnace. The test temperature was controlled at 300°C with two pairs of Type-K thermocouples positioned at the top and bottom grips of the specimen. The tests were performed under a stain controlled mode in a fully reversed condition (R = -1). A high-temperature extensometer mounted on the uniform gauge section of the specimen was used for the strain measurement and feedback control. Instron WaveMatrix^{TM} Dynamic Software was used for the test control and data acquisition. The stress-strain hysteresis loop and the maximum and minimum stresses were recorded at different intervals throughout the test. The number of cycles to failure is defined as the number of cycles when the stress amplitude is reduced by approximately 50% of the maximum stress, or the final recorded cycle when an unstable fracture occurs. Figure 13 shows an example of a fatigue test conducted in air. With the AM sample in its as-printed condition, no cyclic hardening was observed, and the sample experienced cyclic softening throughout the test (Figure 13b-c).

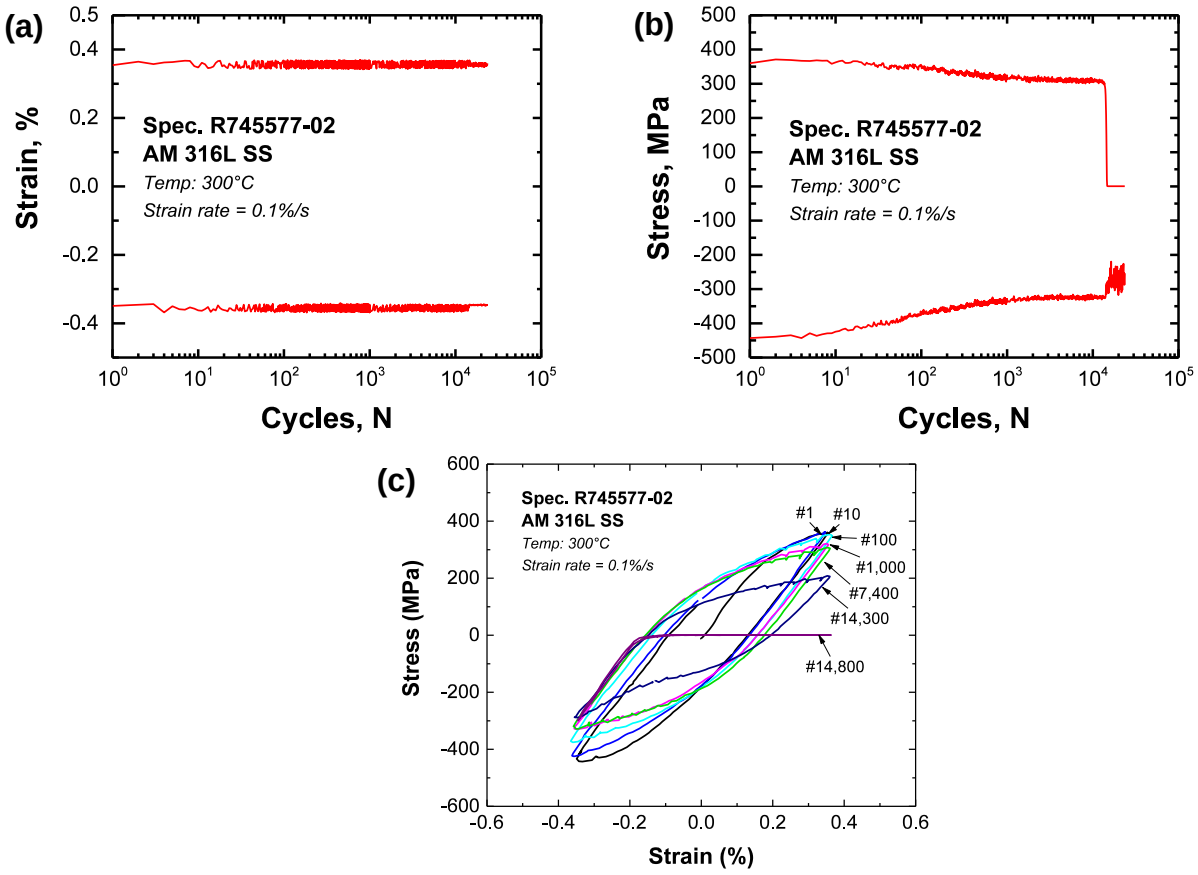

Figure 13 **The strain (a) and stress (b) profiles, and selected hysteresis loops at different cycles (c) for an in-air fatigue test performed at a strain amplitude of 0.35%.**

Fatigue tests in water were performed with a servo-hydraulic test frame retrofitted with an autoclave and a water recirculation system (shown in Figure 14). The autoclave was constructed of Type 316 SS and had an annular volume of ~12 ml around the sample's gauge section. The water circulation system consisted of a 130-liter retention tank, a high-pressure pump, a heat exchanger, and a preheater as shown in Figure 15. During the tests, simulated PWR water was pressurized to ~1450 psig (~10 MPa) and circulated at a rate of ~10 ml/min through the autoclave. The autoclave temperature was controlled at 300°C. Since the extensometer cannot be used inside the autoclave, the in-water tests were conducted by controlling the pull-rod displacement using a linear variable differential transformer (LVDT) located outside the autoclave. The stress-strain results of the in-air fatigue tests were used to determine the input for the pull-rod displacement of the in-water tests. Note that, with this control mode (referred as "stroke control"), the compliance of the load train outside the sample's gauge also influences to the tests. As a result, the applied strain amplitude or strain rate is not constant. However, given the smaller cross-section area of the gauge compared to that of the rest of load train, most of the applied pull-rod displacement should go to the sample gauge. Table 2 shows the fatigue tests performed in air and in PWR water along with their target strain amplitudes (AMP) and strain rates.

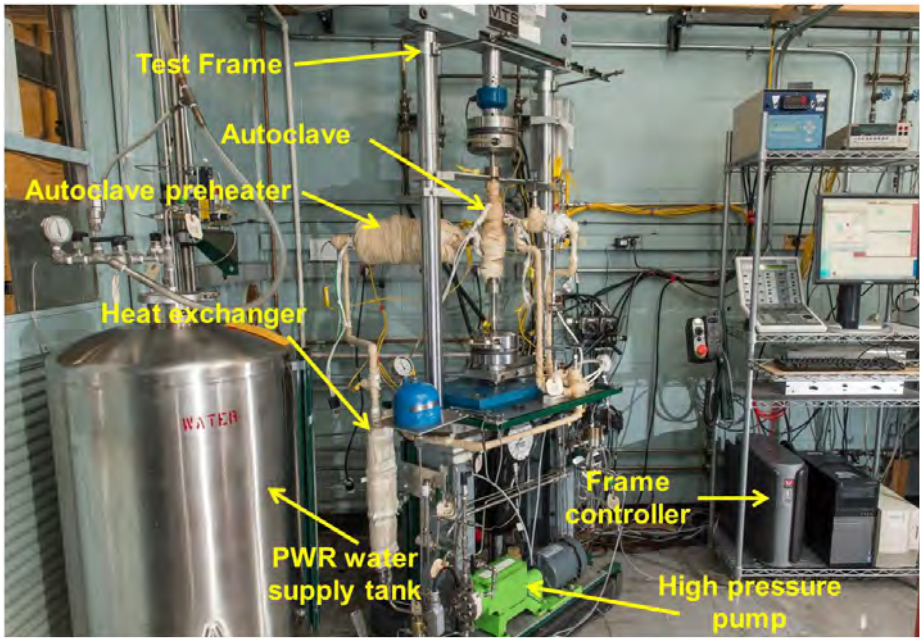

Figure 14 **Fatigue test system equipped with an autoclave and a water circulation system.**

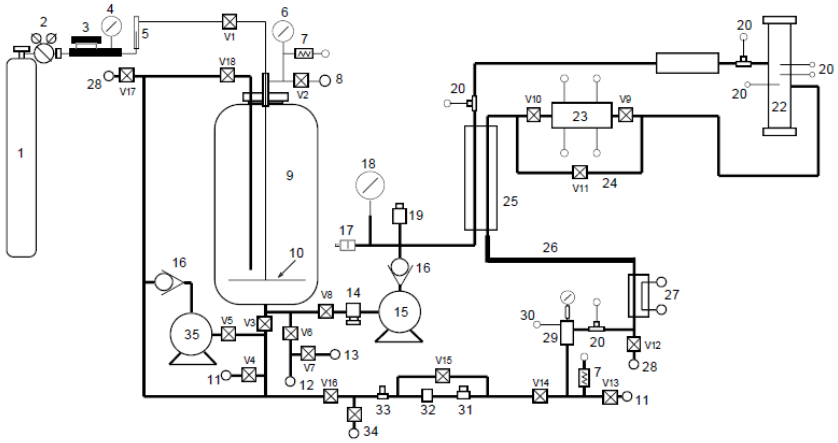

1. COVER GAS SUPPLY TANK
2. HIGH-PRESSURE REGULATOR
3. LOW-PRESSURE REGULATOR
4. PRESSURE GAUGE
5. FLOW METER
6. VACUUM & PRESSURE GAUGE
7. PRESSURE RELIEF VALVE
8. VENT TO ROOM VENTILATION
9. FEEDWATER STORAGE TANK
10. SPARGE TUBE
11. WATER SAMPLE PORT
12. TO 2nd FEEDWATER TANK
13. FEEDWATER FILL PORT
14. SOLENOID VALVE
15. HIGH-PRESSURE PUMP
16. CHECK VALVE
17. RUPTURE DISK
18. HIGH-PRESSURE GAUGE
19. PRESSURE TRANSDUCER
20. THERMOCOUPLE WELL
21. AUTOCLAVE PREHEATER
22. TUBE AUTOCLAVE
23. ECP CELL
24. ECP CELL BYPASS LINE
25. HEAT EXCHANGER
26. LARGER SIZE TUBING
27. WATER COOLED CHILL PLATE
28. SYSTEM BLEED PORT
29. BACK-PRESSURE REGULATOR
30. COMPRESSED AIR LINE
31. CONDUCTIVITY METER
32. PH METER
33. FLOW METER
34. DRAIN
35. RECIRCULATING PUMP
36. RETURN LINE

Figure 15 **Schematic of autoclave water recirculation system for EAF testing.**

Table 2 Fatigue tests conducted in air and in PWR water and their target test conditions

Environment	Test control	Temperature (°C)	Strain AMP (%)	Strain rate (%/s)
Air	Strain	300	0.25	0.1
Air	Strain	300	0.35	0.1
Air	Strain	300	0.45	0.1
PWR water	Stroke	300	0.25	0.1
PWR water	Stroke	300	0.35	0.1

3 Results

This section describes the component-like structures used in this study, the equipment used for microstructural analysis, the configuration of test specimens for CGR testing, and the CGR test apparatus and experimental approach.

3.1 Microstructural characterization

3.1.1 Alloy 316L tubing produced at ANL

The post-build examination consists of visual inspection and optical metallography. The planes of interest were the one susceptible to crack propagation in an actual component.

Crack growth rate measurements are typically made using CT specimens. Figure 16 [16] shows the nomenclature for CT specimen orientations with respect to a cylindrical product form, such as an extruded control rod drive mechanism (CRDM) nozzle or the AM-produced tubing described in this section. The first letter in the two-letter designation is normal to the propagation plane, and the second gives the direction of propagation:

L – direction of maximum grain flow (axial)
R – radial direction, and
C – circumferential or tangential direction

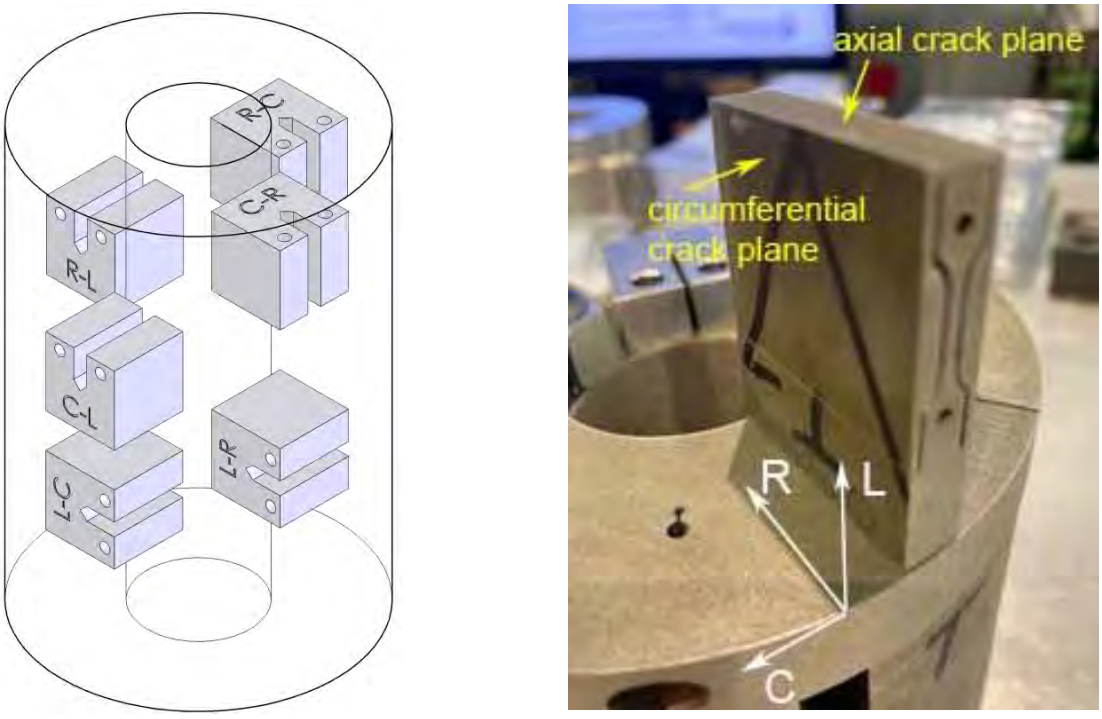

(a) (b)

Figure 16 (a) Specimen orientations for a cylindrical product form [16]; (b) Photograph showing the planes of interest in the AM 316L tubing.

Because cracks in plant components can grow in both length and width, the orientation of an in-service crack propagating through-wall can be represented by the C-R or C-L orientations for an axial crack and by the L-R or L-C orientations for a circumferential crack. The R-L and R-C orientations are parallel to the pressurized surface, often termed the laminar direction; flaws in these orientations have never been observed in service. This is because radial stresses must be in equilibrium with the stress at the surface. The stress at the surface is either zero or compressive and is equal in magnitude to the internal pressure for a pressurized cylinder.

The microstructure in the axial (normal to the build direction) is shown in Figure 17 and the microstructure in the circumferential plane (parallel to the build direction) is shown in Figure 18. Given the build direction, both microstructures were as expected. Porosity was observed, and this will be analyzed with additional accuracy by tomography at ANL APS.

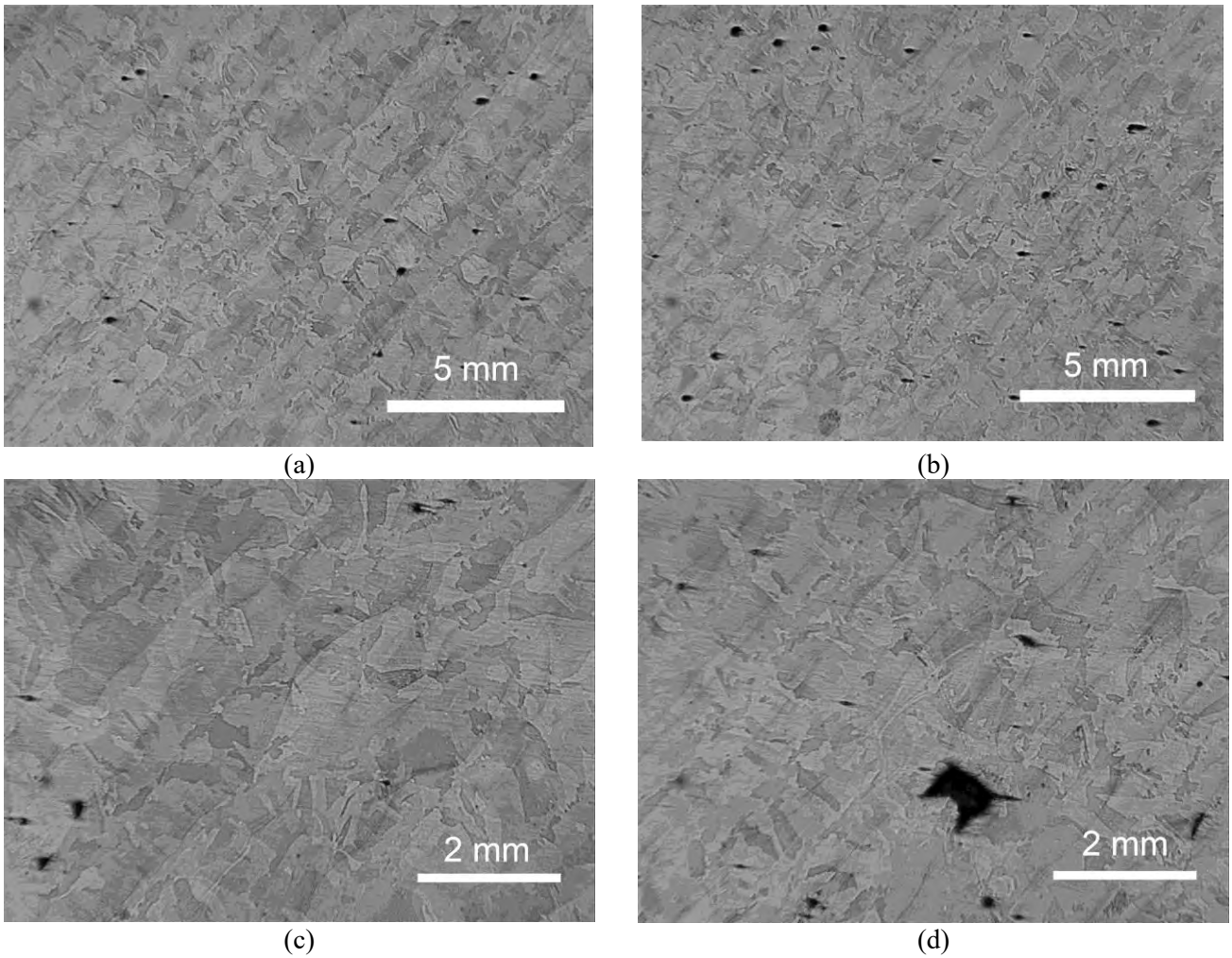

Figure 17 Microstructure in the axial plane (normal to the build direction)

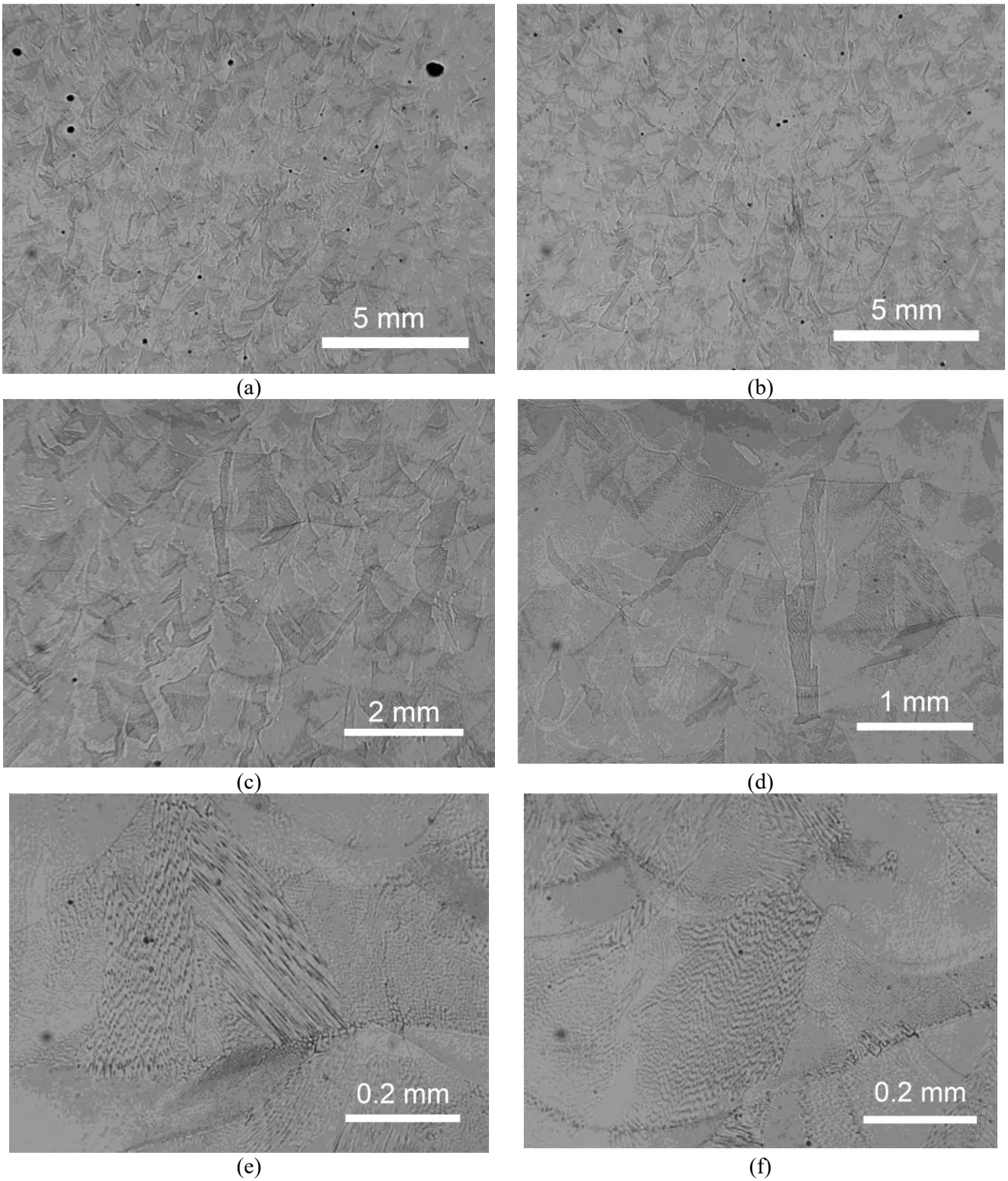

Figure 18 Microstructure in the circumferential plane (parallel to the build direction). Build direction is from bottom to top.

Next, select specimens were studied by SEM-EDS (Scanning Electron Microscopy-Energy Dispersive X-ray Spectroscopy) to quantitatively evaluate the chemical homogeneity and precipitation. In addition, high-energy X-ray tomography – available at Argonne's Advanced Photon Source (APS) was used for a detailed characterization of porosity and micro-cracking, which are critical factors for material's mechanical performance. Figure 19, taken from [17], shows an example of X-ray tomography reconstruction of built-in pores in a LPBF (Laser-Powder Bed Fusion) 316L sample unconnected to this project. The spatial and size distributions of pores can be quantitatively determined. This set of microstructural information should be sufficient to determine the appropriate processing parameters used for printing materials. Subsequent mechanical testing and more detailed microstructural characterization will be used for developing a microstructure-property correlation.

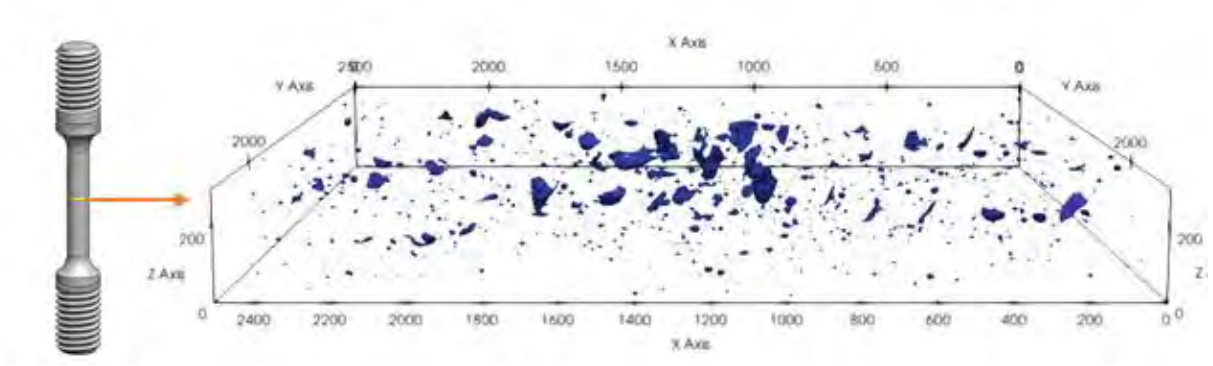

Figure 19 **Synchrotron X-ray tomography of pores in an AM sample; axis labels are in pixel, 1 pix = 4.172 µm. The data from this figure was collected at the Advanced Photon Source at Argonne [17].**

The evaluation of porosity in the as-built material was conducted by X-ray Tomography at Argonne APS, Figure 20. Figure 20a shows the radial bar for porosity measurement, and the arrow indicates the approximate location of the measurement reported here. This was close to the ID of the tube, and representative of the test plane of the CT specimens. The porosity was calculated over a volume of 3.05 mm^3, and was found to be 0.06%, close to the HIP + SA condition described in [9]. The average pore size was 7.2 µm (with a 3 µm detection limit).

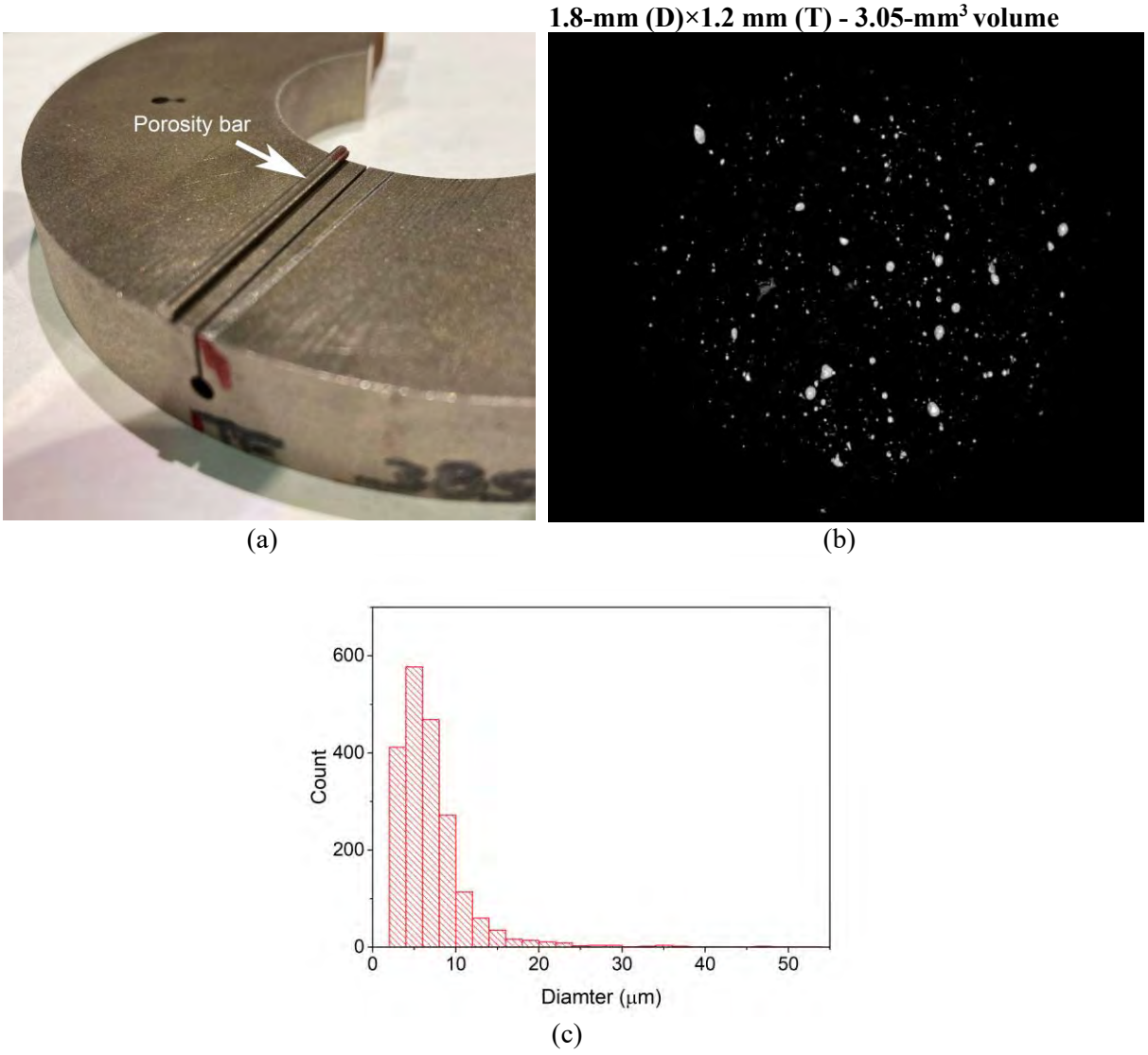

Figure 20 **(a) Radial bar for porosity measurement at ANL APS; arrow indicates the approximate location of the measurement; (b) image showing pores in the bar in a region close to the ID of the tubing in a 3.05 mm³ volume, (c) size distribution of pores.**

3.1.2 Alloy 316L flange produced by industry

The microstructural examination, including porosity will be completed once the ANL APS upgrade is complete.

3.2 SCC Crack growth

SCC CGR testing involved two specimens: B1-CR-1 and B1-CL-1 from the Alloy 316L tubing produced at ANL. The orientations of these specimens with respect to the tubes are shown in Figure 21.

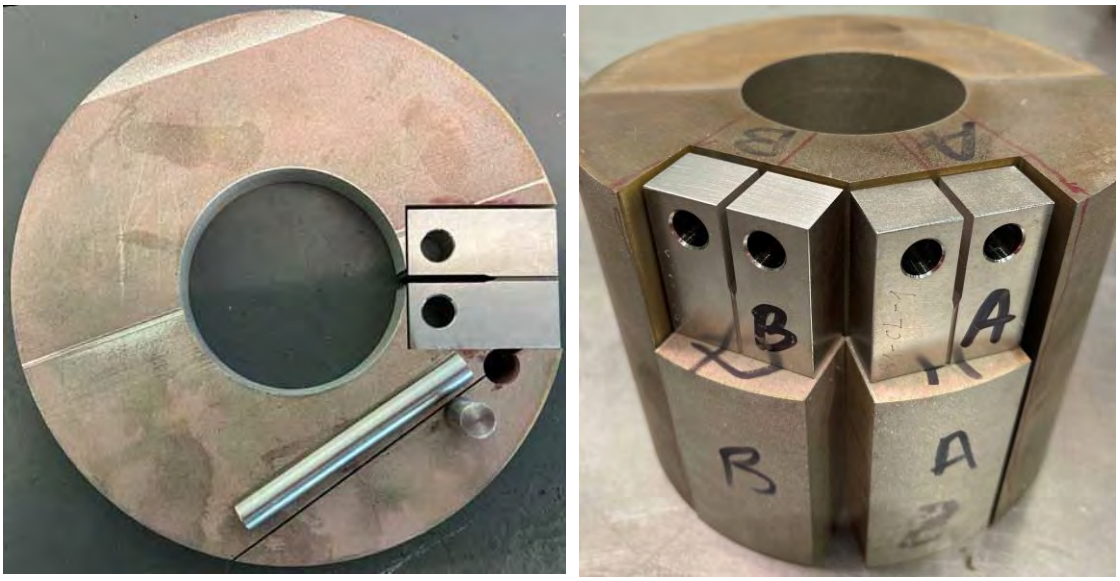

(a) (b)

Figure 21 (a) CT specimen in the CR orientation for SCC CGR testing in LWR environment; (b) CT specimens in the CL orientation for SCC CGR testing in LWR environment.

3.2.1.1 Crack growth rate testing of AM SS316L Specimen B1-CR-1

The testing conditions for specimen B1-CR-1 are given in Table 3, The test was initiated with precracking in the 320°C water environment, and was followed by transitioning (test periods 1-6), and the first SCC CGR determination under constant load in test period 7. The cracking response was low, so the crack was advanced by approximately 1 mm to a new microstructure and the transitioning sequence was repeated. The second SCC CGR determination was made in test period 15, and the SCC CGR response was again low. The overall CGR response, cyclic and SCC, seems to be consistent with that of conventionally-produced alloys.

Table 3 Crack growth data in PWR water[a] for AM 316L Specimen B1-CR-1

Test Period	Test Time, h	Temp. °C	Load Ratio R	Rise Time, s	Down Time, s	Hold Time, s	K_{max}, MPa·m$^{1/2}$	ΔK, MPa·m$^{1/2}$	CGR_{env}, m/s	Estimated CGR_{air}, m/s	Crack Length, mm
Pre a	25	318.4	0.30	1	1	0	25.8	18.0	7.42E-08	7.90E-08	11.981
Pre b	27	318.6	0.30	2	2	0	26.3	18.4	5.89E-08	4.20E-08	12.117
Pre c	28	318.9	0.30	5	5	0	26.7	18.7	3.05E-08	1.77E-08	12.218
1	30	319.0	0.50	120	12	0	26.8	13.4	1.40E-09	3.03E-10	12.240
2	45	318.3	0.50	600	12	0	26.7	13.4	5.19E-10	6.05E-11	12.267
3	51	318.2	0.50	1000	12	0	26.7	13.4	3.70E-10	3.62E-11	12.278
4	70	319.1	0.70	1000	12	0	26.9	8.1	1.59E-10	8.14E-12	12.283
5	141	319.4	0.70	1000	12	7,200	27.0	8.1	5.43E-12	1.01E-12	12.288
6	218	318.9	0.70	1000	12	14,400	27.0	8.1	4.69E-13	5.39E-13	12.289

Table 3 (cont.)

Test Period	Test Time, h	Temp. °C	Load Ratio R	Rise Time, s	Down Time, s	Hold Time, s	K_{max}, MPa·m$^{1/2}$	ΔK, MPa·m$^{1/2}$	CGR_{env}, m/s	Estimated CGR_{air}, m/s	Crack Length, mm
7	680	319.3	1.00	0	0	0	27.0	0.0	9.03E-13	-	12.289
8	683	319.4	0.30	1	1	0	27.0	18.9	9.86E-08	9.26E-08	12.661
9	686	319.9	0.30	2	2	0	28.4	19.9	7.36E-08	5.46E-08	13.009
10	703	319.4	0.50	120	12	0	29.6	14.8	2.68E-09	4.24E-10	13.165
11	728	319.7	0.50	600	12	0	30.3	15.2	8.85E-10	9.19E-11	13.240
12	756	319.7	0.50	1000	12	0	30.8	15.4	6.41E-10	5.78E-11	13.304
13	847	319.9	0.70	1000	12	0	31.0	9.3	1.51E-10	1.31E-11	13.356
14	913	319.6	0.70	1000	12	7,200	31.3	9.4	3.65E-12	1.64E-12	13.369
15	1,472	320.1	1.00	0	0	0	31.6	0.0	no growth	-	13.369

[a]Simulated PWR water with 2 ppm Li, 1000 ppm B as HBO_3, and 2 ppm Li as LiOH. DO<10 ppb. Conductivity was 21±3 μS/cm, and pH 6.4.

3.2.1.2 Crack growth rate testing of AM SS316L Specimen B1-CL-1

The testing conditions for specimen B1-CR-1 are given in Table 4. The test was initiated with precracking in the 320°C water environment, followed by transitioning (test periods 1-6), and the first SCC CGR determination under constant load in test period 7. The response was low, so the crack was advanced by approximately 1.3 mm to a new location and the sequence was repeated. The second SCC CGR determination was made in test period 17. The SCC CGR response in test period 17 over 500 hours at constant load was again low. As with the previous aged specimen, the overall CGR response, cyclic and SCC, seems to be consistent with that of conventionally-produced stainless steels.

Table 4 Crack growth data in PWR water[a] for AM 316L Specimen B1-CL-1.

Test Period	Test Time, h	Temp. °C	Load Ratio R	Rise Time, s	Down Time, s	Hold Time, s	K_{max}, MPa·m$^{1/2}$	ΔK, MPa·m$^{1/2}$	CGR_{env}, m/s	Estimated CGR_{air}, m/s	Crack Length, mm
Pre a	25	319.1	0.30	1	1	0	26.1	18.3	6.45E-08	8.23E-08	11.986
Pre b	27	319.2	0.30	2	2	0	26.2	18.4	4.83E-08	4.19E-08	12.042
Pre c	29	319.3	0.30	5	5	0	26.7	18.7	3.39E-08	1.78E-08	12.171
1	48	319.2	0.50	120	12	0	27.0	13.5	1.90E-09	3.13E-10	12.299
2	55	319.7	0.50	600	12	0	27.1	13.5	6.15E-10	6.32E-11	12.311
3	70	319.8	0.50	1000	12	0	27.1	13.6	4.27E-10	3.82E-11	12.333
4	78	319.7	0.70	1000	12	0	27.1	8.1	1.02E-10	8.39E-12	12.340
5	142	319.6	0.70	1000	12	7,200	27.1	8.1	9.20E-12	1.02E-12	12.348
6	171	319.6	0.70	1000	12	14,400	27.1	8.1	7.20E-12	5.42E-13	12.348
7	480	320.2	1.00	0	0	0	27.1	0.0	no growth	-	12.348
8	483	320.6	0.30	1	1	0	27.4	19.2	1.24E-07	9.68E-08	13.059
9	485	320.8	0.30	2	2	0	30.2	21.1	8.30E-08	6.71E-08	13.251
10	485	320.8	0.30	5	5	0	31.5	22.1	4.57E-08	3.09E-08	13.374
11	503	320.8	0.50	120	12	0	31.3	15.6	3.45E-09	5.10E-10	13.561
12	509	321.0	0.50	600	12	0	32.8	16.4	9.41E-10	1.19E-10	13.583
13	527	321.5	0.50	1000	12	0	32.9	16.4	7.08E-10	7.23E-11	13.630
14	534	321.8	0.70	1000	12	0	33.1	9.9	1.52E-10	1.63E-11	13.635
15	552	321.9	0.70	1000	12	7,200	33.2	10.0	2.69E-11	2.00E-12	13.642
16	647	321.2	0.70	1000	12	14,400	33.4	10.0	1.25E-11	1.09E-12	13.653
17	1,148	321.5	1.00	0	0	0	33.5	0.0	no growth	-	13.654

[a]Simulated PWR water with 2 ppm Li, 1000 ppm B as HBO_3, and 2 ppm Li as LiOH. DO<10 ppb. Conductivity was 21±3 μS/cm, and pH 6.4.

3.3 SCC Crack initiation

3.3.1 Alloy AM 316L CT specimens produced at ANL

3.3.1.1 Crack initiation testing of AM SS316L specimens with the notch pointing up ("UP" specimens)

In this test, two CT specimens printed in a similar orientation, i.e., with the notches pointing up, Figure 22, and differing only at the notch surface – "as printed" vs "machined"- were tested in series in a "faulted", aerated PWR environment. The outcome is shown in Figure 23, and shows that the "as-printed" surface is more likely to initiate and grow a crack than the machined surface.

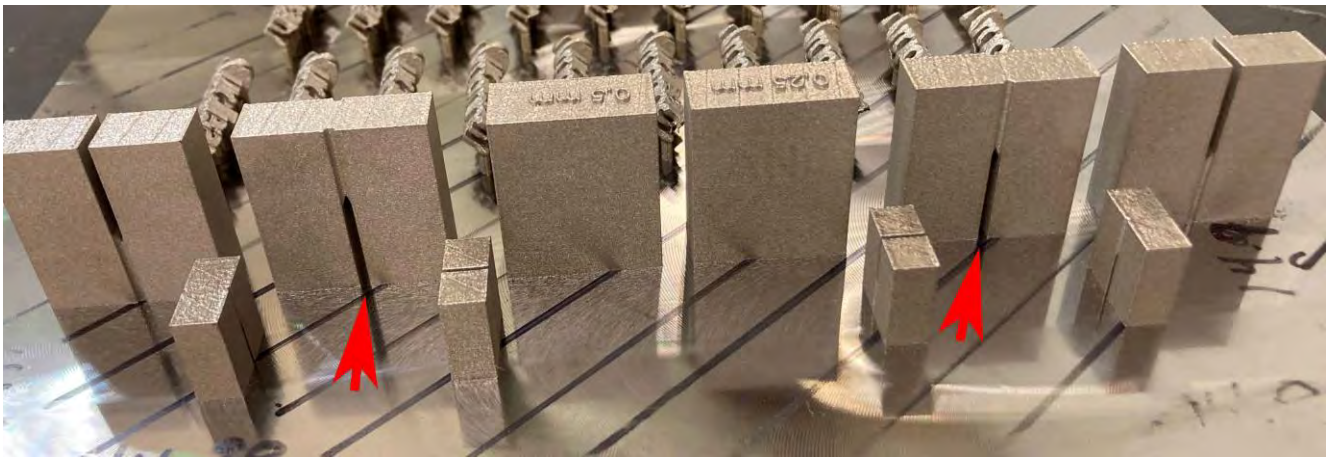

Figure 22 **CGR/crack initiation compact tension specimens printed using the Renishaw AM400 LPBF system. Specimens with similar geometry, printed with the notch "UP", differing only at notch - "as printed" vs "machined" are evaluated for crack initiation simultaneously.**

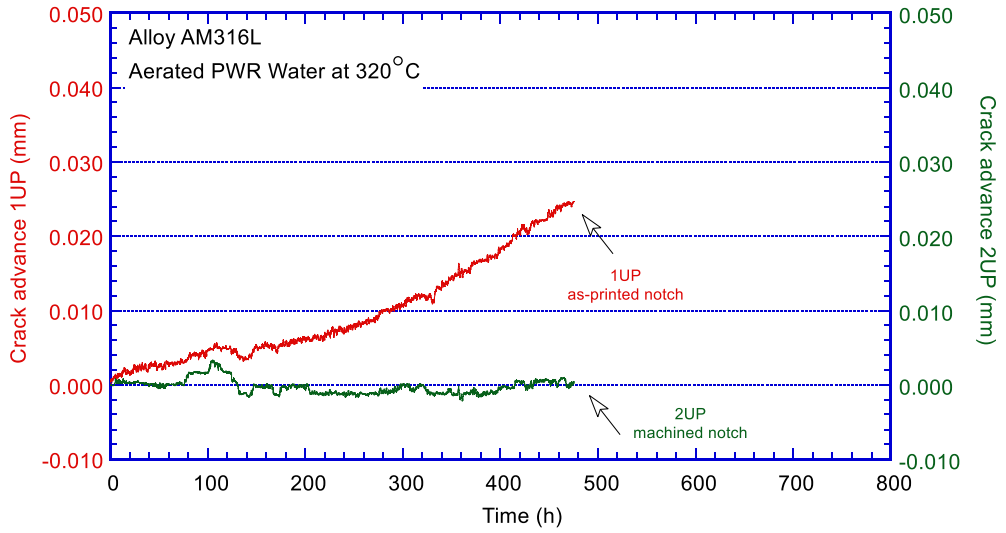

Figure 23 **Crack advance vs. time for AM316L "UP" specimens, printed with the notch up, differing only at notch - "as printed" vs "machined".**

3.3.1.2 Crack initiation testing of AM SS316L specimens with the notch pointing down

In this test, two CT specimens printed in a similar orientation, i.e., with the notches pointing down, Figure 24, and differing only at the notch surface – "as printed" vs "machined"- were loaded in series in a "faulted", aerated PWR environment. The outcome is shown in Figure 25, and shows that after a similar exposure time as the first test, the two specimens printed in this geometry are more resistant to cracking than the specimens printed in the geometry described in the previous section. At the time when this report was written, the test was continuing.

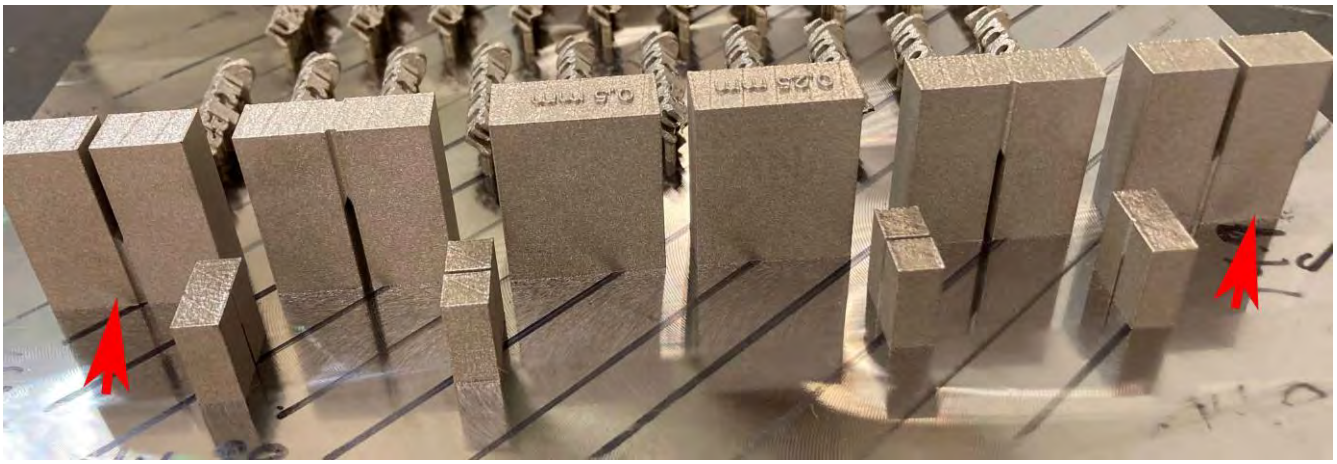

Figure 24 **CGR/crack initiation compact tension specimens printed using the Renishaw AM400 LPBF system. Specimens with similar geometry, printed with the notch "DOWN", differing only at the notch surfaces - "as printed" vs "machined" are evaluated for crack initiation simultaneously.**

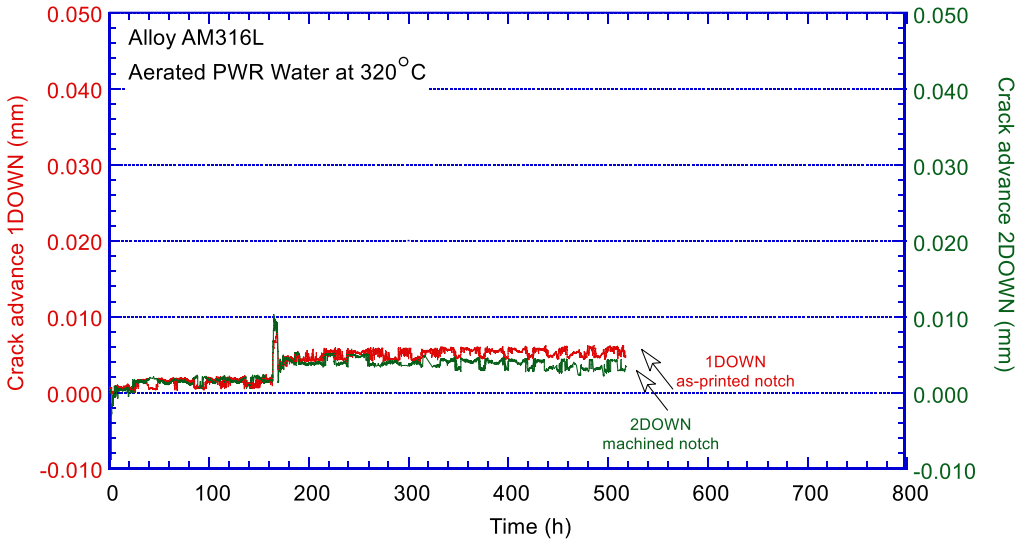

Figure 25 **Crack advance vs. time for AM316L "DOWN" specimens, printed with the notch down, differing only at notch - "as printed" vs "machined" surfaces.**

3.4 Fatigue and Environmentally Assisted fatigue

Three fatigue tests were conducted in air and two in water using the printed AM 316L specimens. Table 5 presents the results obtained from these tests. The temperatures for both the in-air and in-water tests were well controlled, as shown in the table. For the in-air tests, the measured strain amplitude and strain rate were close to the target values (Table 2). For the in-water tests however, since the compliance of the load train changed continuously under the stroke-controlled test mode, average strain amplitudes and strain rates within the sable ranges of the tests were reported in the table. As expected, the fatigue life of AM316L decreases with increasing strain amplitude, and is shorter in water than in air tests.

Table 5 Fatigue tests performed in air and in PWR water

Test ID	Sample ID	Environment	Temperature (°C)	Strain AMP [1] (%)	Strain rate [2] (%/s)	Fatigue life (cycles)
LWRS-01	R745577-01	Air	299	0.25	0.10	42,600
LWRS-02	R745577-02	Air	300	0.36	0.10	14,460
LWRS-03	R745577-03	Air	300	0.46	0.10	4,990
EAF-01	R765768-04	PWR water	298	~0.33	~0.13	6,432
EAF-02	R765768-01	PWR water	299	~0.41	~0.06	2,360

[1, 2] Estimated strain AMP and strain rate for EAF tests in PWR water

3.4.1 Strain-Life Results

The strain-life results obtained on the printed tube are shown in Figure 26a. For comparison, the data points obtained from another AM 316L print by a different laboratory are also included [16]. Both AM prints are tested in their as-printed condition at 300°C. Despite being printed with different LPBF systems and different printing parameters, the two AM heats show a similar trend in the strain-life plot in air. At similar strain amplitudes, fatigue lives of AM316L obtained in water are a factor of two lower than that in air, suggesting an environmental effect on fatigue life in PWR water.

A comparison with wrought SS can be seen in Figure 26b [22, 23]. The fatigue lives of the AM 316L SS in air are slightly lower than that of wrought SSs at ~300°C. However, given the large scatter of fatigue data, the difference are insignificant. For the in-water tests, the data from AM316L are also within the scatter band of wrought SS. Evidentially, the as-printed microstructures of these AM 316L samples do not have a noticeable impact on their fatigue lives in air or in water. Additional data of AM materials are still needed beyond the current range of strain amplitudes to validate this observation.

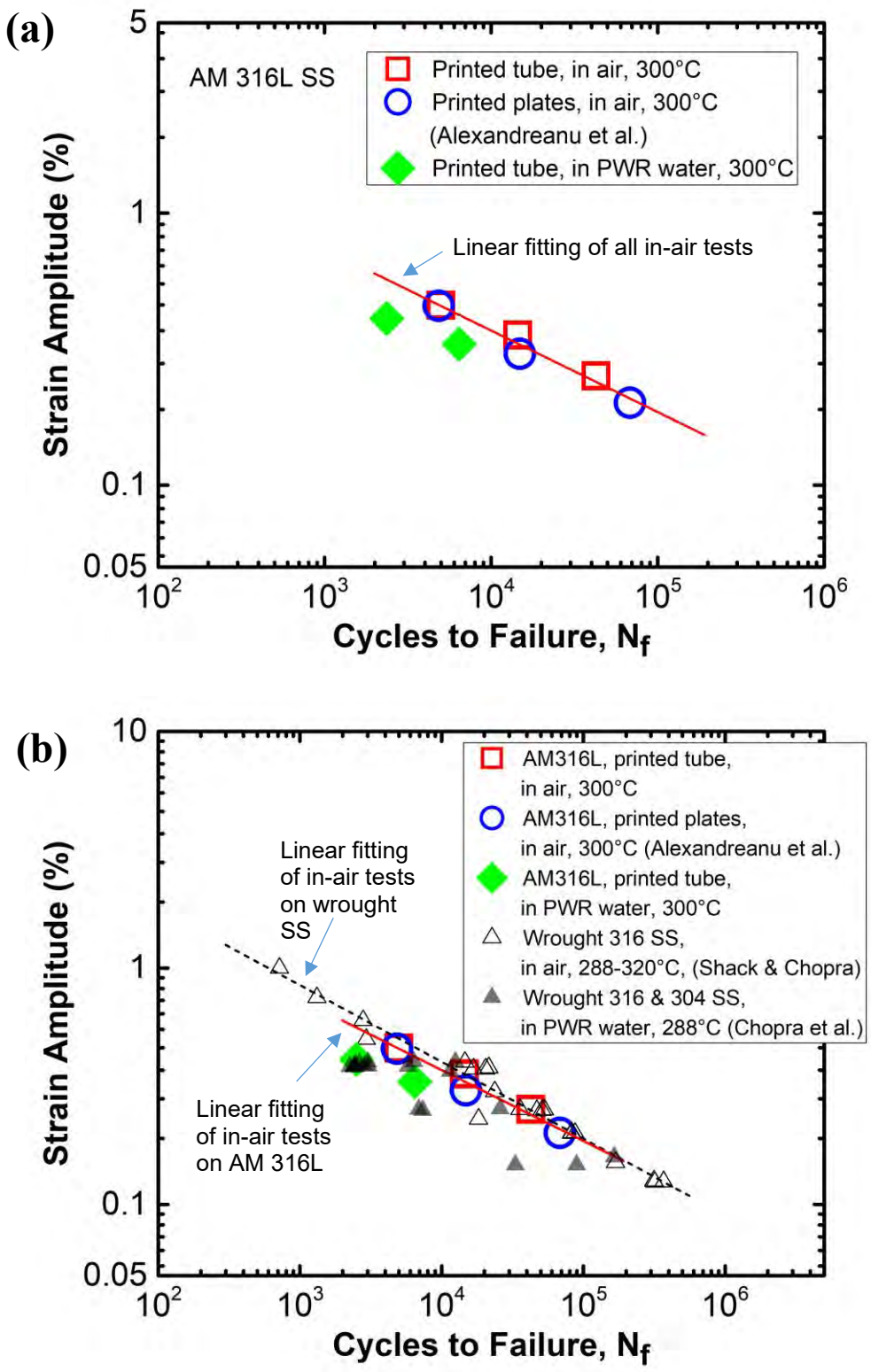

Figure 26 **Strain-life results of (a) AM 316L SS, and (b) comparison of AM 316L and wrought SS at ~300°C [18,19].**

3.4.2 Cyclic Stress Behavior

Figure 27 shows the stress amplitudes as a function of cycles for all tests performed in this study. At 300°C, all specimens behave similarly regardless of their test environments. Cyclic softening dominates the evolution of stress amplitude beyond a brief transient period at the beginning of the cyclic tests. All samples reached their peak stress levels in less than 5 cycles. The cyclic softening may be related to the as-printed condition of these samples since high residual stresses are commonly observed in AM materials without post-built heat treatment. Under cyclic loading, the residual stresses would be relaxed to some extent, leading to cyclic softening. Nonetheless, the stress declines in all tests to a comparable level after ~100 cycles except for the one tested in air at 0.25% strain amplitude. This low-strain-amplitude test also exhibits secondary hardening at the later stage of the test.

For all tests, the initial stress increases with the applied strain amplitude as expected. However, the stress levels for the water tests are somewhat lower than that for the in-air tests at the equivalent strain amplitudes. This is attributed to the different control modes for the in-air and in-water tests. For the in-water test, the displacement of the load train outside the autoclave is controlled. As a result, the strain amplitude evolves within the gauge section of the sample during the test, and the stable stage of the cyclic test was used to estimate the strain amplitude. The actual strain amplitude at the beginning of the test may be lower. Nonetheless, as the test progresses, the cyclic stress responses become stable, and the stress amplitude profiles become similar between the in-air and in-water tests. A long plateau on the strain amplitude profile can be seen for the in-air tests but is absent for the in-water tests, leading to shorter fatigue lives for the in-water tests at equivalent strain amplitudes.

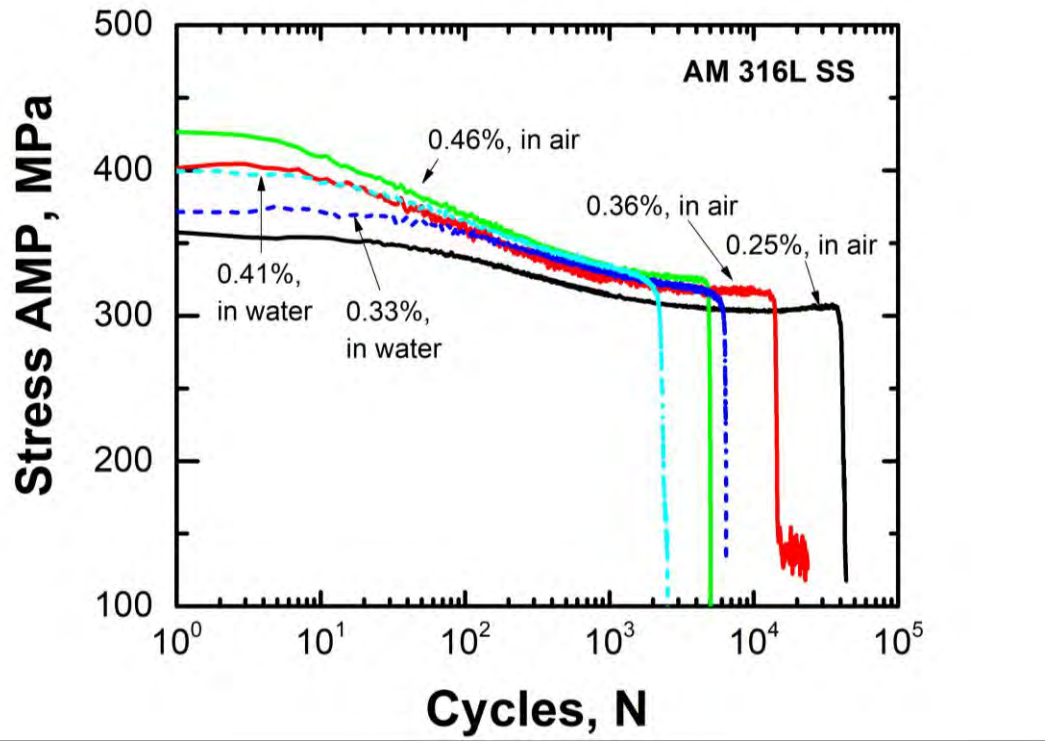

Figure 27 Stress AMP profiles for the in-air and in-water tests at 300°C.

4 Discussion

4.1 Summary of cyclic and SCC CGR data

Figure 28 summarizes the cyclic CGR data for the two AM 316L test specimens. Two sets of data were obtained for each specimen at locations at least 1 mm apart. For comparison, CGR curves developed for wrought alloys by various institutions, such as ANL [18], Paul Sherrer Institut [19], Bettis Laboratory [20] and Japanese Society of Mechanical Engineers (JSME) [21], are included in the figures. One observes that the CGRs for the alloy in the mechanical fatigue regime (10^{-8}-10^{-7} m/s) are exactly as it would be expected for a conventionally-produced alloy, i.e., along the 1:1 diagonal. In the corrosion fatigue regime (10^{-11}-10^{-9} m/s), there is again no difference between the AM alloy and the conventionally-produced SSs. The data shows that the location change – albeit small – did not affect response in either specimen. Also, Figure 28b shows no difference between the two specimens despite their relative orientation vs. build direction. As described previously, both specimens proved to be extremely resistant to SCC. This data demonstrates that the use of AM alloys in a nuclear environment is plausible, however, concerns remain with regard to the heterogeneity and anisotropy of the AM materials.

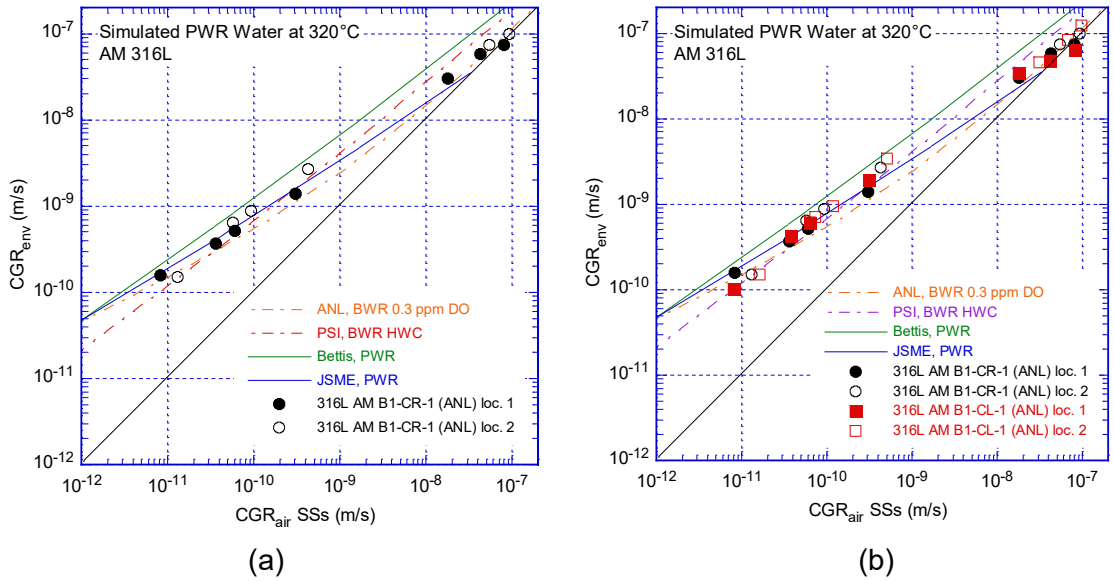

Figure 28 **Cyclic CGRs measured in the PWR environment vs. CGRs predicted in air under the same loading conditions for AM 316L for specimen (a) B1-CR-1, and (b) both B1-CR-1 and B1-CL-1. Also included are CGR curves developed for wrought alloys by various institutions, such as ANL [18], Paul Sherrer Institut [19], Bettis Laboratory [20] and JSME [21]**

Figure 29 shows the SCC CGR data vs K for AM 316L produced at ANL and tested in the as-built condition (porosity 0.06%) as well as data from the literature [9] where AM316L with an initial porosity of 0.3% was post-processed (HIP+SA) to achieve a porosity comparable to that of the ANL material. Also included in the figure are data for wrought and cast SS material along with the NUREG-0313 disposition curve [11]. The comparison shows that AM alloys have a similar response to that of

wrought materials, i.e., the more aggressive NWC (2 ppm DO) results in higher SCC CGRs than that for the deaerated (<5 ppb O) PWR water for alloys with similar porosity. As expected, cold-work by 20% increased the SCC CGR to levels above the NUREG-0313 curve, however, it is not clear that in such cases the desired microstructure is retained. Overall, the SCC CGR response of AM materials seems similar to that of the conventional alloys.

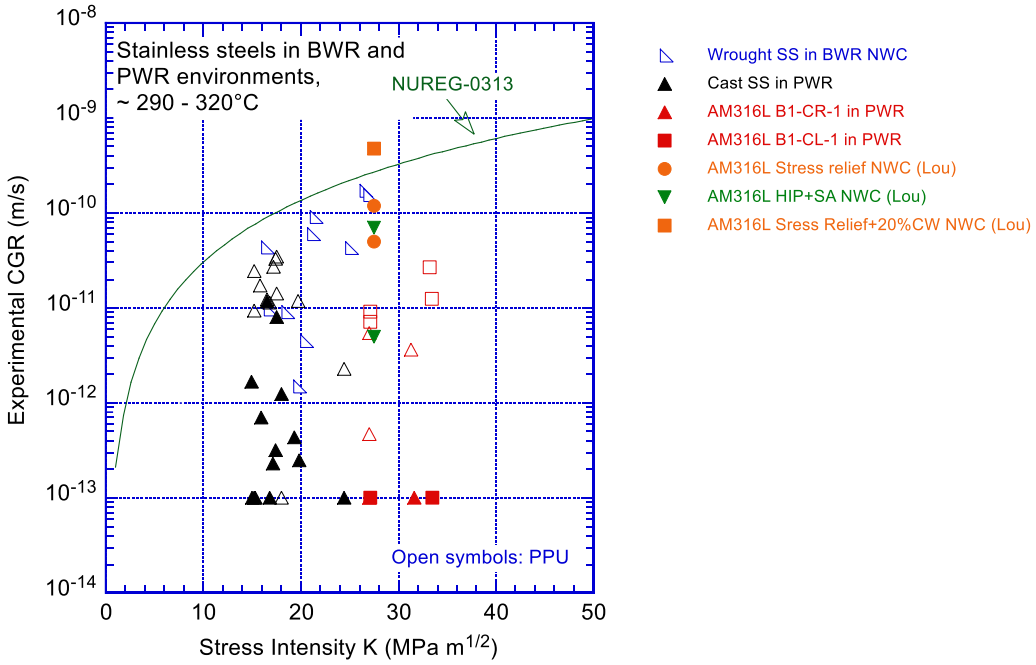

Figure 29 **SCC CGR data vs K for AM 316L for specimen AM316L specimens produced at ANL. (B1-CR-1 and B1-CL-1) and elsewhere [9]. Closed symbols represent data obtained under constant load while open symbols represent data obtained under periodic partial unloading (PPU) conditions. Also included wrought and cast SS data as well as the NUREG-0313 CGR curve.**

4.2 Crack initiation

A comparison between the two crack initiation tests suggest that the specimens printed with the notch pointing down (Figure 23) were more resistant to SCC initiation than the specimens with the notch pointing up (Figure 22). The effect suggests that printing geometry affects local susceptibility to cracking, and the "unsupported" arches such as those of notched pointing up can lead to vulnerabilities. The finding – if supported by future additional observations – suggests that printing unsupported geometries should be avoided. Also, the first test seems to suggest that in cases where susceptibility exists, the as-printed surface initiated cracking faster than the machined surface.

4.3 Environmental assisted fatigue

The ASME Code fatigue design curves, which are based primarily on strain-controlled tests in air, provide the allowable number of cycles as a function of applied stress amplitude. However, the effects of environments on the fatigue performance of materials are not addressed in the ASME fatigue design curves. To incorporate the environmental effects, a correction factor (F_{en}) has been proposed to account for the negative impact of environment on fatigue life [22, 23]. The F_{en} is defined as the ratio of the

fatigue life in air at room temperature to the fatigue life in water at the service temperature. While both fatigue and environmental fatigue data are scarce for AM 316L SS, the same F_{en} approach can be used to assess the environmental effect on AM materials.

Figure 30 shows the strain-life results of AM316L SS and the ASME Code curves developed for wrought austenitic SSs. Within the strain range explored in this study, the data points of the in-air tests (open symbols in the figure) are slightly below the ASME mean curve for wrought SSs. The best fit curve of the AM316L data deviates more from the ASME mean curve with the increase of strain amplitude. Nonetheless, the two data points obtained from the in-water tests are lower than those of the in-air tests, but remain above the ASME Code design curve for wrought SSs.

The F_{en} values of AM 316L samples were estimated with the ASME Code mean curve and the best fit curve to the AM316L tests performed in air at 300°C. As shown in Figure 30, the F_{en} values estimated with the ASME Code mean curve are higher than that estimated with the best fit curve for AM316L data obtained in air. This difference may be attributed to the slightly lower fatigue resistance of AM material compared to its wrought counterpart without a water environment. Since the ASME Code mean curve was developed with wrought SS data, a somewhat higher F_{en} value for AM materials is expected. The F_{en} values estimated with the best fit curve of AM material, though obtained at 300°C, is considered more realistic, since no significant temperature effect is anticipated for austenitic SSs below 400°C in air [22].

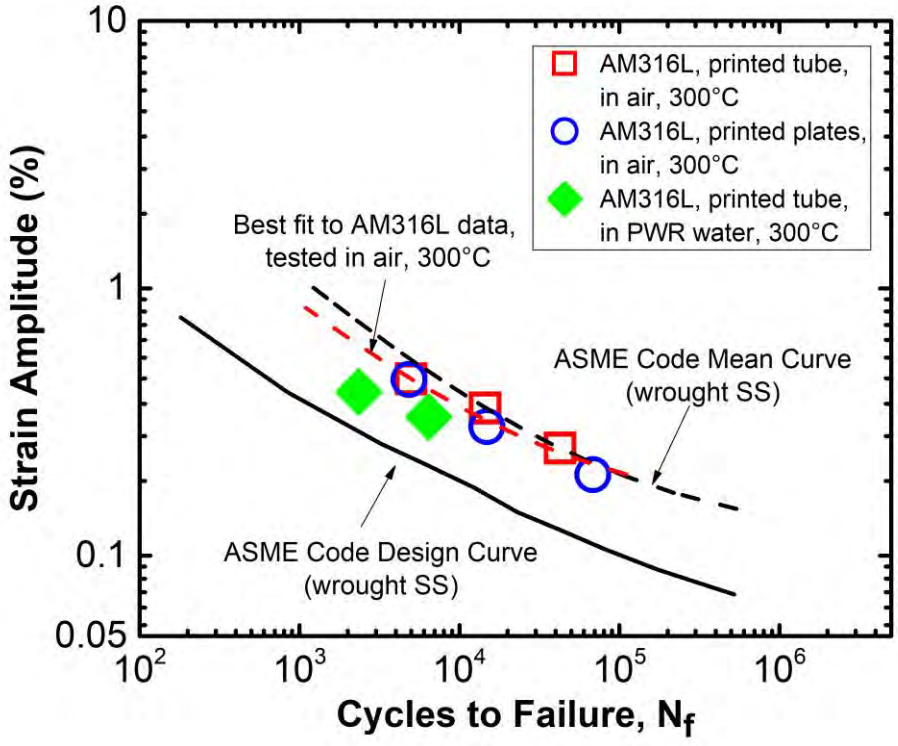

Figure 30 Strain-life data for AM 316L SS compared to ASME Code Mean and Design Curves for wrought SS.

With available data for wrought and cast austenitic SSs, the key material, loading, and environmental parameters influencing the fatigue life were analyzed in NUREG/CR-6909 R1 [23]. A correlation for estimating the fatigue life of wrought and cast SSs in LWR environments was developed, and the F_{en} value of SSs can be expressed as a function the transformed temperature (T*), DO level (O*), and strain rate ($\dot{\varepsilon}^*$),

$$\boldsymbol{F_{en} = \exp(-T^* O^* \dot{\varepsilon}^*)}, \quad (1)$$

where T*, O*, and $\dot{\boldsymbol{\varepsilon}}^*$ are defined as:

$$\begin{aligned} \boldsymbol{T^* &= 0} && \boldsymbol{(T < 100°C)} \\ \boldsymbol{T^* &= (T - 100)/250} && \boldsymbol{(100°C \le T \le 325°C)} \end{aligned} \quad (2)$$

$$\begin{aligned} \boldsymbol{O^* &= 0.29} && \boldsymbol{(DO < 0.1\ ppm)} \\ \boldsymbol{O^* &= 0.29} && \boldsymbol{(DO > 0.1\ ppm,\ \text{sensitized high-carbon SSs})} \\ O^* &= 0.14 && (DO > 0.1\ ppm,\ \text{not sensitized}) \end{aligned} \quad (3)$$

$$\begin{aligned} \dot{\boldsymbol{\varepsilon}}^* &= \boldsymbol{0} && \boldsymbol{(\dot{\varepsilon} > 7\%/s)} \\ \dot{\boldsymbol{\varepsilon}}^* &= \boldsymbol{Ln(\dot{\varepsilon}/7)} && \boldsymbol{(0.0004\%/s \le \varepsilon \le 7\%/s)} \\ \dot{\boldsymbol{\varepsilon}}^* &= \boldsymbol{Ln(0.0004/7)} && \boldsymbol{(\dot{\varepsilon} < 0.0004\%/s)} \end{aligned} \quad (4)$$

With Eqs.(1-4), F_{en} values were calculated for the AM 316L samples tested in PWR water. As shown in Table 6, the obtained F_{en} values are very close to that estimated with the best fit curve of AM material. Evidently, the same F_{en} correlation can be used for AM materials tested in simulated LWR water. Sufficient fatigue tests would still be needed in air at room temperature or below 300°C to establish a reliable mean curve for AM materials without environments. If the in-air fatigue data is insufficient for a sound mean curve, the ASME Code mean curve for wrought SSs can be used to conservatively estimate F_{en} values for AM 316L SS.

Table 6 Estimated environmental correction factor for AM316L SS

Strain AMP (%)	Strain rate (%/s)	Estimated environmental correction factor		
		With the ASME mean curve for wrought SS in air at RT	With the best fit curve to AM316L data in air at 300°C	Estimated based on temperature, DO, and strain rate
~0.33	~0.13	2.8	2.1	2.5
~0.41	~0.07	4.3	2.9	3.0

5 Summary

The performance of AM 316L in simulated water coolant and high temperature air was evaluated. For this purpose, component-like structures were printed, and specimens were machined from these structures. Testing involved SCC initiation, SCC crack growth and EAF. The research and outcomes are summarized as follows:

- Two AM 316L tubes - intended to act as surrogates for complex components where nuclear equipment vendors are more likely to consider AM technologies - were printed at ANL using a Renishaw AM400 LPBF system. The porosity of the as-built material was found to be small, 0.06%.
- The fatigue and corrosion fatigue CGR response of two AM specimens in the as-built condition - oriented normal to and parallel to the build direction - was found to be similar to that expected for conventional alloys. Also, both AM specimens in the as-built condition proved to be extremely resistant to SCC. This data demonstrates that the use of AM alloys in a nuclear environment is plausible.
- Crack initiation tests suggest that printing geometry affects local susceptibility to cracking, i.e., "unsupported" arches such as those of notched pointing up can lead to vulnerabilities. The finding – if supported by future additional observations – suggests that printing unsupported geometries should be avoided. Also, initial testing seems to suggest that in cases where susceptibility exists, the as-printed surface initiated cracking faster than the machined surface.
- Strain-controlled fatigue tests in air were conducted with 3D-printed 316L SS under different strain amplitudes in a fully reversed mode. The fatigue lives of AM 316L were slightly lower than that of traditionally made 316 SS, especially at high strain amplitudes. For the tests performed in simulated PWR water, the fatigue lives of AM316L were lower than that obtained in air, suggesting a negative impact of LWR environments on AM materials. Cyclic softening dominates the evolution of stress amplitude for all fatigue tests on AM 316L SS both in air and in water. The cyclic softening may be related to the as-printed condition of these samples since high residual stresses are commonly observed in AM materials without post-built heat treatments.
- Following the same approach proposed in NUREG-6909 for wrought and cast austenitic SSs, environmental correction factors, F_{en}, were estimated for AM316L tested at different strain amplitudes with the ASME Code mean curve and the best fit curve to the in-air test data on AM316L SS. The estimated F_{en} values are reasonably close, suggesting a similar baseline behavior in air for wrought and AM316L SSs. With the correlation developed for wrought SSs in NUREG-6909, similar F_{en} values can be obtained for AM316L using key parameters influencing environmental fatigue, such as temperature, DO level in water, and strain rate.

References

1. International Energy Agency. 2019. Nuclear Power in a Clean Energy System, https://www.iea.org/reports/nuclear-power-in-a-clean-energy-system.
2. U.S. Energy Information Administration. 2021. "Primary Energy Production by Source." accessed August 30, 2021. Sourced from: https://www.eia.gov/totalenergy/data/browser/.
3. Electric Power Research Institute, 2021. Leveraging Existing Infrastructure – Nuclear Power, Paper for Summer Seminar 2021
4. K.A. Terrani "Accelerating the Deployment of Advanced Nuclear Energy Systems." Nuclear News, Apr. 2020, 34-37.
5. Roadmap for Regulatory Acceptance of Advanced Manufacturing Methods in the Nuclear Energy Industry, Nuclear Energy Institute, May 13, 2019.
6. D.W. Gandy, Strategy/approach for qualification of nuclear components produced via additive manufacturing, in: US DOE Advanced Methods of Manufacturing Workshop, US Department of Energy, Germantown, MD, USA, 2016.
7. A. Hiser, NRC Perspectives on Advanced Manufacturing Technologies, GAIN Advanced Manufacturing for Nuclear Workshop, December 4, 2018.
8. M. Audrain, NRC Technical Assessment of Additive Manufacturing –Laser Powder Bed Fusion, NRC Workshop on Advanced
9. Xiaoyuan Lou, Miao Song, Paul W. Emigh, Michelle A. Othon, Peter L. Andresen, "On the stress corrosion crack growth behavior in high temperature water of 316L stainless steel made by laser powder bed fusion additive manufacturing", Corrosion Science, 128, pp 140-153, 2017
10. Xiaoyuan Lou, Michelle A. Othon, Raul B. Rebak, "Corrosion fatigue crack growth of laser additively-manufactured 316L stainless steel in high temperature water", Corrosion Science, 127, pp 120-130, 2017.
11. W.S. Hazelton, "Technical report on material selection and processing guidelines for BWR coolant pressure boundary piping", NUREG-0313-Rev2, 1986.
12. American Society for Testing and Materials, "Standard Test Method for Measurement of Fatigue Crack Growth Rates," ASTM E647-08, DOI 10.1520/E0647-08, West Conshohocken, PA, 2008.
13. American Society for Testing and Materials, "Standard Test Method for Determining a Threshold Stress Intensity Factor for Environment-Assisted Cracking of Metallic Materials," ASTM E1681-03, DOI 10.1520/E1681-03R08, West Conshohocken, PA, 2008.
14. Electric Power Research Institute, "PWR Primary Water Chemistry Guidelines," Volume 1, Revision 4, EPRI, Palo Alto, CA, 1999.
15. American Society for Testing and Materials, "Standard Test Method for Strain-Controlled Fatigue Testing," ASTM E606/E606M-21, DOI:10.1520/E0606_E0606M-21, West Conshohocken, PA, 2021.
16. Alexandreanu, B., X. Zhang, Y. Chen, W.-Y. Chen and M. Li. "Mechanical Testing of Additively Manufactured Materials."Argonne National Laboratory, ANL/NSE-22/83, 2022.
17. M. Li, X. Zhang, W.Y. Chen, T.S. Byun, Creep behavior of 316 L stainless steel manufactured by laser powder bed fusion, J. Nucl. Mater., 548 (2021), Article 152847.
18. Shack, W. J., and T. F. Kassner, "Review of Environmental Effects on Fatigue Crack Growth of Austenitic Stainless Steels," NUREG/CR–6176, ANL–94/1, May 1994.
19. H.P. Seifert and S. Ritter, Environmentally-Assisted Cracking in Austenitic Light Water Reactor Structural Materials, PSI Bericht Nr. 09-03, March 2009, ISSN 1019-0643.
20. G.F. Li, J. Congleton, *Corrosion Science*, 42, pp. 1005 – 1021, 2000.

21. S.L. Hong et al., "Measurements of stress corrosion cracking growth rates in weld Alloy 182 in primary water of PWR", Proc. of the 10th Int. Conf. on Environmental Degradation of Materials in Nuclear Power Systems – Water Reactors, Houston, TX: NACE, 2001, CDROM.
22. O. K. Chopra, and Shack, W. J., 1998, “Effects of LWR Coolant Environments on Fatigue Design Curves of Carbon and Low-Alloy Steels,” NUREG/CR-6583, ANL-97/18.
23. O. K. Chopra, and G. L. Stevens, “Effect of LWR Coolant Environments on the Fatigue Life of Reactor Materials—Final Report,” NUREG/CR-6909. Rev.1, May 2018.

This page intentionally left blank

Nuclear Engineering Division
Argonne National Laboratory
9700 South Cass Avenue, Bldg. 208
Argonne, IL 60439

www.anl.gov